PI31 is an adaptor protein for proteasome transport in axons

Kai Liu[1], Sandra Jones[1], Adi Minis[1], Jose Rodriguez[1], Henrik Molina[2], Hermann Steller[1,3,*]
[1]Strang Laboratory of Apoptosis and Cancer Biology, The Rockefeller University, 1230 York Avenue, New York, NY 10065, USA.
[2]The Rockefeller University Proteomics Resource Center, The Rockefeller University, New York, NY, 10065, USA
[3]Lead contact
*Correspondence: steller@rockefeller.edu.

Abstract
Degradation of proteins by the ubiquitin-proteasome pathway (UPP) is critical for the maintenance of protein homeostasis, cell function and survival. While all cells require regulated protein degradation, nerve cells face unique challenges as their highly complex structure and large intracellular space requires special mechanisms to allocate proteasomes to appropriate sub-cellular compartments where protein breakdown occurs. Here we show that the conserved proteasome-binding protein PI31 mediates axonal transport of proteasomes. PI31 binds directly to both proteasomes and dynein light chain LC8-type proteins (DYNLL1/2) and thereby promotes the formation of DYNLL1-PI31-proteasome complexes both *in vivo* and *in vitro*. Inactivation of PI31 inhibits proteasome motility in axons of *Drosophila* neurons, similar to ablation of *dDYNLL1/ctp*, and it disrupts synaptic protein homeostasis, structure and function. These results indicate that PI31 serves a critical function as an adapter protein to transport proteasomes to the periphery of neurons via microtubule-based motors. Because mutations affecting the activity of PI31 are associated with human neurodegenerative diseases, it is possible that impairment of PI31-mediated axonal transport is the root cause of these disorders.

Introduction

Protein homeostasis (proteostasis) is essential for cellular and organismal health (Balch et al., 2008; Glickman and Ciechanover, 2002; Goldberg, 2003; Varshavsky, 2005). Eukaryotic cells have two major systems for clearing unwanted, damaged and potentially toxic proteins: the ubiquitin-proteasome pathway (UPP) and the autophagy-lysosome system(Eskelinen and Saftig, 2009; Glickman and Ciechanover, 2002; Goldberg, 2003; Kenney and Benarroch, 2015; Martini-Stoica et al., 2016; Pan et al., 2008; Tai and Schuman, 2008). The UPP carries out the degradation of the vast majority of intracellular proteins, whereas autophagy is primarily responsible for the removal of protein aggregates and damaged organelles. In the UPP, proteins are tagged for destruction by the linkage of multiple copies of ubiquitin. The actual degradation of proteins in the UPP is carried out by multi-subunit protease particles termed 26S proteasomes(Baumeister et al., 1998; Collins and Goldberg, 2017; Glickman and Ciechanover, 2002). The 26S proteasomes consist of 20S core particles, which contain the active proteases, and 19S regulatory subunits(Collins and Goldberg, 2017). It has been suggested that proteasomes are typically present in excess and that their capacity is not fully used, at least in the absence of stress(Asano et al., 2015). On the other hand, some cell types appear to require special mechanisms to position proteasomes to appropriate sub-cellular compartments where protein breakdown occurs. This is especially important for neurons, since they are very large, structurally complex and highly compartmentalized cells that require transport mechanisms to allocate proteasomes to sites distant from the cell body (Bingol and Sheng, 2011; Tai and Schuman, 2008). Proteasome function is required for the growth and pruning of both axons and dendrites during development (DiAntonio et al., 2001; Erturk et al., 2014; Kuo et al., 2005; Wan et al., 2000; Watts et al., 2003). Moreover, in mature neurons UPP-mediated protein degradation at synapses is critical for activity-dependent plasticity, learning and memory(Bingol and Sheng, 2011; Callow et al., 2011; Campbell and Holt, 2001; Davis et al., 1992; Hegde et al., 2014; Lee et al., 2008; Pak and Sheng, 2003; Patrick, 2006; Yi and Ehlers, 2005). Recently, proteasomes were found to insert into the plasma membrane of neurons and acutely regulate synaptic activity and calcium signaling(Ramachandran and Margolis, 2017). Due to the considerable distances from the soma, neurons employ microtubule-based transport mechanisms to deliver proteasomes to the periphery of neurons(Bingol and Schuman, 2006; Hsu et al., 2015; Kreko-Pierce and Eaton, 2017). However, despite the critical function of proteasomes at synapses, much remains to be learned about the underlying transport mechanisms. CamKIIα-dependent phosphorylation of the proteasome subunit Rpt6 is one mechanism to recruit proteasomes into dendritic spines, where excitatory postsynaptic densities are harbored, in response to neuronal depolarization(Bingol and Schuman, 2006; Bingol et al., 2010; Djakovic et al., 2009). This also directly links neuronal activity with local proteasome regulation, since CamKIIα can be activated by calcium entry through NMDA receptors in depolarized neurons. On the other hand, the mechanisms regulating proteasome transport in axons and their localization to the presynaptic regions are less clear. One of the molecular motors, the dynein complex, plays a key role in motility of proteasomes in axons(Hsu et al., 2015; Kreko-Pierce and Eaton, 2017). A recent study identified dynein light chain LC8-type proteins (DYNLL1/2) as important components of microtubule-dependent proteasome transport in *Drosophila* neurons and demonstrated

that this process is distinct from the movement of synaptic vesicles(Kreko-Pierce and Eaton, 2017). However, a central unresolved question is how exactly proteasomes are coupled to microtubule-based motor complexes.

Here we show that the conserved proteasome-binding protein PI31 ("proteasome inhibitor of 31kD") mediates fast axonal transport of proteasomes in *Drosophila* motor neurons by acting as an adapter between proteasomes and dynein light chain LC8-type proteins. PI31 was originally identified based on its ability to inhibit 20S-mediated hydrolysis of peptides *in vitro* (Chu-Ping et al., 1992; McCutchen-Maloney et al., 2000; Zaiss et al., 1999). On the other hand, work in *Drosophila* has shown that inactivation of PI31 impairs protein degradation during sperm maturation, and that PI31 can stimulate the proteolytic capacity of cells by promoting the assembly of 19S and 20S particles into the fully active 26S proteasome(Bader et al., 2011; Cho-Park and Steller, 2013). Similarly, the PI31 ortholog in yeast, Fub1, is required to alleviate proteotoxic stress (Yashiroda et al., 2015). However, studies in cultured HEK293 mammalian cells have failed to reveal a clear effect of PI31 for proteasome activity, suggesting that PI31 function may be different in different cell types and systems (Li et al., 2014).

PI31 also binds directly and strongly to the F-box protein Ntc/Fbxo7/PARK15, and this interaction is conserved from *Drosophila* to mammals(Bader et al., 2011; Kirk et al., 2008). Interestingly, mutations in FbxO7/PARK15 impair proteasome function and cause a juvenile form of Parkinson's Disease (PD) in humans and PD-like symptoms in mice(Conedera et al., 2016; Di Fonzo et al., 2009; Paisan-Ruiz et al., 2010; Vingill et al., 2016). Since many age-related neurodegenerative diseases, including Alzheimer's Disease (AD) and PD, are characterized by the accumulation of protein aggregates, it is possible that mutations in FbxO7/PARK15 impair the clearance of pathological proteins (Ballatore et al., 2007; Irvine et al., 2008; Li and Li, 2011; Oddo, 2008; Ross and Poirier, 2004; Tai and Schuman, 2008). F-box proteins serve as substrate recognition modules in multi-component E3-ligase complexes for UPP-mediated protein degradation (Bai et al., 1996; Kipreos and Pagano, 2000; Skaar et al., 2013; Skowyra et al., 1997). However, very unexpectedly for an E3 ligase, binding of FbxO7 to PI31 does not result in PI31 degradation but rather serves to protect PI31 from proteolytic cleavage (Bader et al., 2011; Vingill et al., 2016). These observations are consistent with the idea that loss of FbxO7 leads to impaired proteasome through inactivation of PI31, but direct evidence for this model is lacking due to insufficient knowledge about the precise function of PI31 in neurons. In order to address these questions, we more carefully investigated the consequences of PI31 inactivation in *Drosophila*. In addition to the previously reported defects in spermatid differentiation, we found a striking requirement of PI31 in neurons, and specifically for synaptic structure and function. Focusing on motor neurons as a model, loss of PI31 function reduced the numbers of presynaptic active zones and caused defects in protein homeostasis in the periphery of neurons. Significantly, we identified *Drosophila* homologs of dynein light chain LC8-type proteins (dDYNLL1/Ctp and dDYNLL2/Cdlc2) as direct binding partners of PI31. PI31 can directly interact with both dDYNLL1/Ctp and proteasomes *in vitro*, and it can promote the binding of proteasomes to dDYNLL1/Ctp. Inactivation of PI31 blocks proteasome motility in axons and produces a phenotype very similar to the inactivation of dDYNLL1/Ctp(Kreko-Pierce

and Eaton, 2017). The interaction of PI31 and DYNLL1/2 is conserved from *Drosophila* to mammals, indicating that this function is conserved. Collectively, these findings indicate that PI31 is a direct adaptor protein to load proteasome onto dynein complexes and thereby mediates axonal transport of proteasomes.

Results

Requirement of PI31 for neuronal function and synaptic structure

PI31 is a conserved proteasome-binding protein, and its expression is enriched in heads and testes in *Drosophila*, suggesting its functions are crucial for these organs(Bader et al., 2011; Chintapalli et al., 2007; Cho-Park and Steller, 2013; McCutchen-Maloney et al., 2000; Yashiroda et al., 2015). Consistently, knockout of PI31 in testes leads to the proteotoxic stress and abnormal development of sperms(Bader et al., 2011). To study the role of PI31 in neurons, we used the R94G06-GAL4 to drive the expression of UAS-HA-PI31, and examined its localization in neurons. R94G06-GAL4 only expresses in one motor neuron (MN1-IB) on each hemi-segment of *Drosophila* larval ventral nerve cord, the axon of which targets Muscle 1 (Figure S1). We found that PI31 forms puncta along axons and in neuromuscular junctions (NMJs) (Figure 1A), suggesting it may have a local function there.

Local activity of proteasomes plays a key role in turnover of synaptic proteins and regulates the growth, strength, activity and plasticity of synapses (Bingol and Schuman, 2006; DiAntonio et al., 2001; Ding et al., 2007; Djakovic et al., 2009; Ehlers, 2003; Erturk et al., 2014; Hegde et al., 2014; Kuo et al., 2005; Speese et al., 2003; Willeumier et al., 2006). As a proteasome-binding protein that forms puncta in axons and NMJs, PI31 may promote local protein degradation there. To study this possibility, we conducted immunofluorescence studies to compare the amounts of poly-ubiquitinated proteins (Poly-Ub), the substrates of proteasomes, in axons and NMJs of wild-type and *PI31*$^{-/-}$ larvae. Quantification of these results demonstrates that *PI31*$^{-/-}$ larval axons contained significantly more Poly-Ub puncta compared to wild-type axons (Figure 1B and 1C). Consistently, the intensity of Poly-Ub staining in Muscle 4 (M4) NMJs was also elevated (Figure 1D and 1E). These data indicate that the loss of PI31 impairs protein degradation in axons and synapses, and they suggest that PI31 has a critical role in regulating proteasome abundance or activity in nerve terminals.

Since local activity of UPP is important for the growth and maintenance of NMJs (DiAntonio et al., 2001; Valakh et al., 2012; Wan et al., 2000), we examined NMJ anatomy of wild-type and *PI31*$^{-/-}$ larvae. For this purpose, we conducted immunofluorescence analyses using Brp and HRP antibodies to label presynaptic active zones and neuronal membranes respectively, and analyzed M4 NMJs (Figure S2A and 1F) and Muscle 6/7 (M6/7) NMJs (Figure S2B and S2C). Although the overall morphology of NMJs was similar between wild-type and *PI31*$^{-/-}$ larvae (Figure S2A and S2B), the number of presynaptic active zones was significantly reduced in *PI31*$^{-/-}$ larvae (Figure 1F, 1G, and S2C). In particular, we found that the number of small-volume synapses (<0.5 μm^3) was dramatically reduced in *PI31*$^{-/-}$ larvae, whereas big-volume synapses (>0.5 μm^3)

appeared not affected (Figure 1H). Our results indicate that PI31 is required to maintain proper synaptic morphology at the NMJ.

To examine whether the synaptic defects reflect a cell autonomous requirement for PI31, we used the mosaic analysis with a repressible cell marker (MARCM) to inactivate PI31 in a limited number of cells (Wu and Luo, 2006) (Figure S2D and 1I). *PI31*$^{-/-}$ neurons are marked by GFP expression, whereas the GFP-negative neurons are *PI31*$^{+/-}$ and serve as an internal control. Quantification of Brp puncta indicates that *PI31*$^{-/-}$ neurons have reduced number of presynaptic active zones (Figure 1I and 1J). This is consistent with the results from PI31 full knockout larvae (Figure 1F and 1G). Interestingly, co-staining of MARCM M4 NMJs with Brp and GluRIIC antibodies, which label presynaptic active zones and postsynaptic densities respectively, shows that some synapses in *PI31*$^{-/-}$ neurons had reduced presynaptic active zones but maintained postsynaptic densities (Figure 1K and 1L, indicated by white arrowheads). A previous report demonstrated that knockdown of proteasome subunits in motor neurons results in similar changes of synapses (Valakh et al., 2012), suggesting that the synaptic defects of *PI31*$^{-/-}$ neurons are due to insufficient proteasome activity in synapses. The presence of postsynaptic densities also indicates that the reduction of presynaptic active zones is a synaptic maintenance defect, rather than a developmental or growth defect.

We also inactivated PI31 in neurons with a neuron-specific driver, *nrv2-GAL4*. *nrv2>PI31 RNAi* homozygotes died as pharate adults that appeared overall well-developed. These mutants initiated but did not complete the eclosion process as they displayed a strong leg motor defect that made it impossible for them to escape from pupal cases (Table S1). Taken together, these results indicate that inactivation of PI31 leads to proteotoxic stress in axons and synapses, which in turn causes structural and functional synaptic defects.

Dynein light chain LC8-type proteins are binding partners of PI31

To understand the mechanism by which PI31 promotes proteostasis in the periphery of neurons, we looked for new binding partners of PI31. For this purpose, we expressed N-terminal HA-tagged PI31(HA-PI31) in flies and performed anti-HA co-immunoprecipitation (Co-IP) followed by label-free quantitative mass spectrometry (MS). Since HA-PI31 rescued the lethality of PI31 knockout flies, we conclude that the N-terminal tag did not interfere with PI31 functions(Bader et al., 2011). Results from this analysis revealed that all 20S proteasome subunits were highly enriched in the ani-HA-PI31 Co-IP, compared to the control Co-IP, which did not include HA-PI31 (Figure 2). This is consistent with previous studies, and suggests our Co-IP-MS method reflects the interactome of PI31 *in vivo*(Bader et al., 2011; Cho-Park and Steller, 2013; McCutchen-Maloney et al., 2000; Yashiroda et al., 2015). These Co-IP experiments were performed in the absence of ATP, which is required for the stability of 26S particles(Liu et al., 2006). Therefore, the failure to detect interactions of PI31 with 19S proteasomes in these experiments does not mean that PI31 is only in a complex with 20S proteasomes (see Figure S4C). Interestingly, among the statistically most significant proteins, we noticed two dynein light chain LC8-type proteins, Ctp (*Drosophila* homolog of dynein light chain LC8-type 1, dDYNLL1) and Cdlc2 (*Drosophila* homolog of dynein light chain LC8-type

2, dDYNLL2) (Figure 2). Both proteins consist of 89 amino acids, share 98.9% identity, and differ in only one amino acid (Figure S3A). Since both unique peptides were identified by MS, this suggests that both proteins can bind to PI31 (Figure S3B). Significantly, dDYNLL1/Ctp was recently shown to be responsible for axonal transport of proteasomes in *Drosophila* motor neurons(Kreko-Pierce and Eaton, 2017). This raises the possibility that PI31 may involve in axonal transport of proteasomes as well.

dDYNLL1/Ctp directly interacts with PI31

In order to confirm the interaction between PI31 and dDYNLL1/2, we performed Co-IP-Western blot assays. HA-PI31 was able to pull down dDYNLL1/2 in both S2 cells and transgenic flies (Figure S4A and 3A), indicating the existence of a PI31-dDYNLL1/2 complex *in vivo*. To avoid possible overexpression artifacts and examine the interaction of PI31 and dDYNLL1 under endogenous expression levels, we inserted a HA-tag into the N-terminus of the genomic locus of PI31 in frame with its coding sequence by CRISPR-Homology Directed Repair (HDR). The expression level of HA-PI31$^{\text{Knock-in}}$ was comparable to PI31 levels in wild-type flies (Figure 3B). Using this system to conduct anti-HA Co-IP experiments, we were able to show that PI31 can pull down dDYNLL1/2 and proteasomes at physiological levels of protein expression (Figure 3B).

To provide additional evidence for the interaction of PI31 and dDYNLL1/2, we also performed the reciprocal Co-IP using FLAG-dDYNLL1 as the bait and found it to successfully pull down PI31 (Figure 3C). Finally, to investigate whether PI31 and dDYNLL1/Ctp directly interact with each other, we expressed GST-PI31 and FLAG-dDYNLL1 recombinantly in *E. coli,* and conducted GST-pull down assays. This revealed that GST-PI31 can pull down FLAG-dDYNLL1, whereas GST alone cannot (Figure 3D). We conclude that PI31 is a direct binding partner of dDYNLL1/Ctp.

Dynein motor complexes are highly conserved in evolution(Hirokawa et al., 2010; Schliwa and Woehlke, 2003; Vale, 2003). In order to investigate whether the interaction between PI31 and dynein light chain LC8-type proteins is conserved in mammals, we performed Co-IP experiments in both MEFs and HEK293 cells. Using GFP-tagged mouse PI31 (GFP-mPI31) and HA-tagged human PI31 (HA-hPI31), we found that PI31 interacted with DYNLL1/2 in both cell types (Figure 3E and S4B). Taken together, these findings indicate that mammalian PI31 directly interacts with DYNLL1/2 proteins, and that this interaction is conserved from *Drosophila* to mammals.

Previous work showed that PI31 binds directly to 20S proteasomes (Bader et al., 2011; Cho-Park and Steller, 2013; Chu-Ping et al., 1992; McCutchen-Maloney et al., 2000; Yashiroda et al., 2015). However, whether PI31 is in a complex with 26S proteasomes is less clear (Yashiroda et al., 2015). To address this question, we used again HA-PI31$^{\text{Knock-in}}$ flies. This time, anti-HA Co-IP experiments were conducted in the presence of ATP to preserve 26S proteasomes and interacting proteins were eluted under native conditions. Our results indicate that PI31 interacts with both 20S proteasomes and single-capped 26S proteasomes *in vivo* (Figure S4C). On the other hand, double-capped 26S proteasomes were not captured by this approach, suggesting that PI31 cannot bind to

them efficiently (Figure S4C). Based on these results, it is possible that PI31 is involved in the transport of both 20S and single-capped 26S proteasomes.

dDYNLL1/Ctp forms a protein complex with proteasomes

Since PI31 can directly bind to both dDYNLL1/Ctp and proteasomes, we explored the idea that this protein may serve as an adapter to promote formation of a multi-protein complex containing proteasome and dynein. In order to look for evidence of such a complex, we expressed FLAG-dDYNLL1 in S2 cells and conducted the anti-FLAG Co-IP experiments to see if proteasomes can be pulled down. Through MS analysis, we identified most of the 20S proteasome subunits. This confirmed the existence of a dDYNLL1/Ctp-proteasome complex (Figure 4A). Interestingly, PI31 was among the statistically most significant binding partners of dDYNLL1/Ctp, providing additional support for the relevance of this interaction. We further confirmed the existence of the dDYNLL1/Ctp-proteasome complex by Co-IP-Western blot assays using an antibody against the 20S proteasome subunit α7 (Figure 4B).

PI31 promotes the formation of dDYNLL1/Ctp-proteasome complex

If PI31 is an adaptor protein mediating the formation of dDYNLL1/Ctp-proteasome complexes, increased amounts of PI31 should facilitate complex formation. To test this possibility, we expressed HA-PI31 with FLAG-dDYNLL1 in S2 cells, performed anti-FLAG Co-IP experiments, and compared the amount of proteasomes pulled down by FLAG-dDYNLL1 with or without HA-PI31. These experiments demonstrate that elevated levels of PI31 can indeed increase the amount of proteasomes bound to dDYNLL1/Ctp (Figure 5A).

To confirm that this effect is due to direct interactions mediated by PI31, we reconstituted the complex *in vitro* using purified 20S proteasomes and recombinant GST-PI31 and FLAG-dDYNLL1from *E.coli*. Firstly, FLAG-dDYNLL1 was bound to anti-FLAG-magnetic beads. Then, 20S proteasomes were added alone, or with GST, or GST-PI31. This approach showed that GST-PI31 was able to load 20S proteasome onto dDYNLL1/Ctp, whereas 20S proteasome alone or with GST did not bind to dDYNLL1/Ctp (Figure 5B). Taken together, these results show that PI31 is a direct adaptor protein that promotes the formation of a complex between proteasomes and dDYNLL1/Ctp.

PI31 is required for the axonal transport of proteasomes in motor neurons

Our results so far suggest that PI31 may mediate axonal transport of proteasomes by promoting the formation of DYNLL1/2-proteasome complexes. To examine a requirement of PI31 for this process, we used a recently established proteasome reporter system, UAS-Prosβ5-RFP, for live-imaging of proteasome movement in axons of *Drosophila* larval motor neurons(Kreko-Pierce and Eaton, 2017). This is a very elegant and powerful system since Prosβ5-RFP is incorporated into functional proteasomes when expressed in motor neurons(Kreko-Pierce and Eaton, 2017). For these studies, expression of the reporter in motor neurons was driven by R94G06-GAL4 (Figure S1). Using this assay, we found that inactivation of PI31 significantly reduced motility of axonal proteasomes (Figure 6A-C, and Movie S1 and S2). In wild-type larva, 30.5% of proteasome particles exhibited anterograde movement with an average velocity of 0.71±

0.06 μm/s; 44.1% of proteasome particles exhibited retrograde movement with an average velocity of 0.42±0.03 μm/s; the remaining 25.4% of proteasome particles either appeared stationary or moved randomly within the time frame of live imaging (Figure 6 A-C and Movie S1). These results are consistent with previous analyses of proteasome transport in axons of *Drosophila* motor neurons(Kreko-Pierce and Eaton, 2017). Next, we examined the movement of proteasome particles in *PI31*$^{-/-}$ larva. In this case, both anterograde and retrograde movement of proteasomes was severely reduced: 82.0% of proteasome particles remained stationary or moved randomly, and only 8.6% and 9.5% of proteasome particles displayed anterograde and retrograde movement, respectively (Figure 6A-C and Movie S2). Moreover, the small number of moving proteasome particles in *PI31*$^{-/-}$ larva had significantly reduced velocities (Figure 6C). These phenotypes are remarkably similar to the defects of proteasome transport reported in *dDYNLL1/ctp*$^{-/-}$ larva(Kreko-Pierce and Eaton, 2017). Therefore, we conclude that PI31 is required for fast transport of proteasomes along motor neuron axons.

Since PI31 interacts with proteasomes and dynein light chain LC8-type proteins in both *Drosophila* and mammals, we explored the possibility that the function of PI31 as an adapter to mediate axonal transport of proteasomes is conserved in evolution. As a first step, we examined the subcellular localization of PI31 and proteasomes in axons of cultured mouse dorsal root ganglion (DRG) neurons. For this purpose, we transfected primary DRG neuron cultures with mouse proteasome subunit α4-mCherry and mCerulean-mPI31 and conducted live-imaging analyses (Movie S3). The results of these experiments show that α4-mCherry and mCerulean-mPI31 co-localize and move together along DRG axons (Figure 6D and 6E, and Movie S3). These observations are consistent with the idea that the function of PI31 as an adapter to mediate axonal transport of proteasomes has been conserved to mammals.

Discussion

The degradation of unwanted and potentially toxic protein by the ubiquitin-proteasome pathway (UPP) is of critical importance for protein homeostasis. In addition, UPP-mediated protein degradation also sculpts cell shape during normal development and modifies tissues throughout life. Examples include the terminal differentiation of spermatids, loss of muscle mass in response to starvation, dendritic pruning of nerve cells, and the maturation and modification of synapses to mediate neuronal plasticity(Bader et al., 2011; Campbell and Holt, 2001; Hegde et al., 2014; Lecker et al., 1999; Lee et al., 2008; Pak and Sheng, 2003; Patrick, 2006; Qian et al., 2013; Sandri, 2013; Watts et al., 2003; Yi and Ehlers, 2005; Zhong and Belote, 2007). Neurons pose a particular challenge for regulated protein degradation due to their large size and highly compartmentalized structure. The importance of localized regulation of UPP activity is crucial for synaptic growth, strength, plasticity and maintenance(Bingol and Schuman, 2006; DiAntonio et al., 2001; Djakovic et al., 2012; Ehlers, 2003; Hamilton and Zito, 2013; Kuo et al., 2005; Ramachandran and Margolis, 2017; Speese et al., 2003; Wan et al., 2000; Watts et al., 2003; Zhao et al., 2003). Nerve cells employ microtubule-based transport mechanisms to deliver proteasomes to the periphery of neurons(Bingol and Schuman, 2006; Hsu et al., 2015; Kreko-Pierce and Eaton, 2017). However, despite the critical function of proteasomes at synapses, much remains to be learned about the underlying transport mechanisms. A recent report showed that dynein light chain LC8-type proteins (DYNLL1/2) are important components of microtubule-dependent proteasome transport in *Drosophila* neurons and demonstrated that this process is distinct from the movement of synaptic vesicles(Kreko-Pierce and Eaton, 2017). In this study, we identified the very same dynein light chain proteins as direct binding partners of the conserved proteasome regulator PI31 ("Proteasome *I*nhibitor of 31kD"). Because PI31 binds directly to proteasomes, the ability of PI31 to also bind to DYNLL1/2 proteins suggests that PI31 serves as an adapter to couple proteasomes via dynein light chain proteins to microtubule-based motors(Bader et al., 2011; Cho-Park and Steller, 2013; Chu-Ping et al., 1992; Li et al., 2014; McCutchen-Maloney et al., 2000; Yashiroda et al., 2015; Zaiss et al., 1999). In support of this idea, inactivation of PI31 disrupted proteasome movement in *Drosophila* neurons and caused functional and structural neuronal defects. In particular, *PI31*$^{-/-}$ neurons had reduced presynaptic active zones, and mosaic analysis demonstrates that this reflects a cell-autonomous requirement for PI31 in neurons. Furthermore, loss of PI31 function led to the accumulation of Poly-Ub aggregates at nerve terminals and in axons, consistent with the idea that insufficient amounts of proteasomes were available in the periphery of neurons for proper protein degradation. Collectively, our results suggest that PI31 is a direct adaptor for microtubule-dependent transport of proteasomes in axons and thereby promotes allocation of proteasomes to synapses (Figure 7).

Our results may help reconcile somewhat conflicting reports in the literature. PI31 was initially identified as a proteasome-interacting protein, and binding of PI31 to 20S particles can inhibit peptide proteolysis *in vitro*(Bader et al., 2011; Chu-Ping et al., 1992;

McCutchen-Maloney et al., 2000; Zaiss et al., 1999). On the other hand, genetic studies in both yeast and *Drosophila* indicate that the physiological function of PI31 is to promote protein breakdown(Bader et al., 2011; Yashiroda et al., 2015). It is also worth noting that PI31 activity is subject to post-translational modification, and that large cells, such as spermatids and neurons are particular sensitive to the loss of PI31 (Bader et al., 2011; Cho-Park and Steller, 2013). In contrast, no overt requirements for PI31 were detected in cultured HEK293 cells, and PI31-inactivation produces only modest biochemical changes at the level of whole-cell extracts(Cho-Park and Steller, 2013; Li et al., 2014). The mechanism reported here provides an explanation for these seemingly conflicting reports as it reveals a role of PI31 for localized regulation of proteasomes. Such a localized function is not readily detectable by standard methodologies for assessing proteasome activity in whole-cell extracts.

The results presented here may also have important implications for human neurological disorders. Many age-related neurodegenerative diseases, including Alzheimer's Disease (AD) and Parkinson's Disease (PD), are characterized by the accumulation of protein aggregates(Ballatore et al., 2007; Irvine et al., 2008; Li and Li, 2011; Oddo, 2008; Ross and Poirier, 2004; Tai and Schuman, 2008). The proteins in these pathognomonic aggregates are typically ubiquitin-conjugated (de Vrij et al., 2004; Mori et al., 1987; Morimoto, 2008; Morishima-Kawashima et al., 1993; Perry et al., 1987; Rubinsztein, 2006). This suggests that the affected neurons attempted to remove abnormal proteins by tagging them with ubiquitin, but subsequently failed to degrade them. One possible explanation for this is that proteasomes were not available in sufficient numbers to degrade all ubiquitin-conjugates. Because the first signs of impaired proteostasis and accumulation of pathological proteins are generally seen in the periphery of neurons, it has been suggested that defects in proteasome transport may be responsible for abnormal protein clearance in neurodegenerative diseases(Coleman and Perry, 2002; Gendron and Petrucelli, 2009; Hoover et al., 2010; Ittner et al., 2010; Otero et al., 2014; Yoshiyama et al., 2007; Yu and Lu, 2012). PI31 is implicated in this process since human mutations affecting PI31 activity are associated with neurodegenerative diseases, including AD, PD and amyotrophic lateral sclerosis (ALS)(Aguado et al., 2010; Conedera et al., 2016; Di Fonzo et al., 2009; Johnson et al., 2010; Koppers et al., 2012; Paisan-Ruiz et al., 2010; Sherva et al., 2011). Perhaps the most compelling case for linking PI31 with human disease comes from the analysis of FbxO7/PARK15 mutants. Mutations in this gene lead to an early, familiar form of PD in humans, and inactivation of FbxO7 in mice causes neuronal degeneration and PD-like phenotypes (Conedera et al., 2016; Di Fonzo et al., 2009; Paisan-Ruiz et al., 2010; Vingill et al., 2016). FbxO7 is a strong and direct binding partner of PI31 in both insects and mammals, and loss of FbxO7 function results in proteolytic cleavage and reduced levels of PI31(Bader et al., 2011; Kirk et al., 2008). Strikingly, FbxO7-Null mice were found to have significantly reduced PI31 levels, but a critical function of PI31 was dismissed based on analysis of whole-cell extracts(Vingill et al., 2016). Since a role of PI31 in axonal transport would

not have been detected by this approach, we suggest that this topic deserves further investigation.

Methods

Fly husbandry and strains

All flies were raised on standard molasses formulation food at 25°C with a 12-hour light/12-hour dark cycle. The following fly strains were used: *R94G06-GAL4* (Janelia GAL4 collection) (Pfeiffer et al., 2008), *UAS-mCD8-mCherry* (Bloomington Drosophila Stock Center, BDSC #27392), *UAS-HA-PI31*(Bader et al., 2011), *PI31*$^{-/-}$(Bader et al., 2011), *hsp70-FLP*^{1}, *FRT42D tubP-GAL80* (BDSC #9917), *D42-GAL4* (BDSC # 8816), *UAS-IVS-myr::GFP* (BDSC #32197)(Pfeiffer et al., 2010), *tubP-GAL4* (BDSC # 5138), *tubP-GAL80*^{ts} (BDSC #7018), *nrv2-GAL4 UAS-GFP* (BDSC #6794), *UAS- PI31 RNAi*^{KK105476} (Vienna Drosophila Resource Center, #105476) and *UAS-Prosβ5-RFP*(Kreko-Pierce and Eaton, 2017) (kindly provided by Dr. Benjamin A. Eaton, University of Texas).

Fly genotypes for each figure are listed below:

Figure 1A. *w; UAS-HA-PI31/+; R94G06-GAL4/+*.

Figure 1B-G and Figure S2A-D. WT: *yw; +/+; +/+*.

PI31$^{-/-}$: *w; PI31*$^{\Delta}$*/PI31*$^{\Delta}$*;+/+*.

Figure 1H-K. *yw, hsp70-FLP*^{1}*; FRT42D, tubP-GAL80/FRT42D, PI31*$^{\Delta}$*; UAS- IVS-myr::GFP/D42-GAL4*.

Figure 2 and Figure 3A. Control: *yw; +/+; tubP-GAL4, tubP-GAL80*^{ts} */+*.

HA-PI31: *w; UAS-HA-PI31/+; tubP-GAL4, tubP-GAL80*^{ts}*/+*.

Figure 3B. and Figure S4C. Control: *yw; +/+; +/+*.

HA-PI31$^{Knock\text{-}in}$: *w; HA-PI31*$^{Knock\text{-}in}$*/ HA-PI31*$^{Knock\text{-}in}$ *; +/+*.

Figure 5A-C. WT: *w; +/+; R94G06-GAL4, UAS-Prosβ5-RFP/R94G06-GAL4, UAS-Prosβ5-RFP*.

PI31$^{-/-}$: *w; PI31*$^{\Delta}$*/ PI31*$^{\Delta}$*; R94G06-GAL4, UAS-Prosβ5-RFP/R94G06-GAL4, UAS-Prosβ5-RFP*.

Figure S1. *w; +/+; R94G06-GAL4/UAS-mCD8-mCherry*.

Table S1. nrv2-GAL4: *w;+/+; nrv2-GAL4, UAS-GFP/nrv2-GAL4, UAS-GFP*.

PI31 RNAi: *w; PI31 RNAi*^{KK105476}*/PI31 RNAi*^{KK105476}.

nrv2>PI31 RNAi: *w; PI31 RNAi*^{KK105476}*/PI31 RNAi*^{KK105476}*; nrv2-GAL4, UAS-GFP/nrv2-GAL4, UAS-GFP*.

Constructs

The gRNA construct for making HA-PI31$^{Knock\text{-}in}$ fly was generated by annealing of two ssDNA oligonucleotides (ssODN) (F_GTCGAGTCGACCCACTTTCCATTG; R_AAACCAATGGAAAGTGGGTCGACT) together and insertion of the annealed product into the BbsI site of pCFD3-dU6:3gRNA vector(Port et al., 2014) (a gift from Dr. Simon Bullock, Addgene#49410).

The HA-PI31 fragment was cut from pcDNA3-HA-PI31(Bader et al., 2011) using EcoRI and XhoI (New England Biolabs). FLAG-dDYNLL1 was cloned from a yw

cDNA library by PCR and the FLAG-tag sequence was added on the forward primer in frame with the dDYNLL1 coding sequence (CDS). HA-PI31(EcoRI/XhoI) and FLAG-dDYNLL1(EcoRI/XbaI) fragments were inserted into the S2-cell expression vector pAc5.1/V5-His-A(Thermo Fisher Scientific, V411020).

The HA-PI31 fragment was cut from pcDNA3-HA-PI31(Bader et al., 2011) using EcoRI and XhoI and inserted into the pGEX-4T1 vector (GE Healthcare, #28954549) to generate pGEX-4T1-PI31 clone. FLAG-dDYNLL1 fragment was generated by PCR using pAc5.1A-FLAG-dDYNLL1 as the template, digested with NcoI and EcoRI (New England Biolabs), and inserted into pET28a vector (Novagen, #69864-3) to generate the pET28a-FLAG-dDYNLL1 clone.

Mouse PI31 (mPI31) CDS was cloned from a cDNA library of mouse small intestine, which was generated by Superscript III First Strand Synthesis Kit (Thermo Fisher Scientific, #18080051) using oligo(dT) amplification, and inserted into the BstI/XmaI sites of pLVX-EF1a-AcGFP-C1 vector (Clontech, #631984). The lentivirus was packaged by transfection of pLVX-EF1a-AcGFP-C1-mPI31, pMD2.G (a gift from Dr. Didier Trono, Addgene #12259) and psPAX2 (a gift from Dr. Didier Trono, Addgene #12260) into HEK293 cells, and collected 48 hours after transfection. Human PI31 (hPI31) CDS was cloned from a cDNA library of HEK293 cells, and inserted into pcDNA3.2/V5/GW/D-TOPO vector (Thermo Fisher Scientific, K244020) through TOPO cloning method (kindly provided by Dr. Park Cho-Park, University of Pennsylvania).

Mouse proteasome subunit α4 CDS was cloned from a mouse cDNA library, and mCherry CDS was subcloned from the mCherry-Mito-7 vector (Olenych et al., 2007) (a gift from Dr. Michael Davidson, Addgene #55102). The α4-mCherry cassette was inserted between the EcoRI/NotI sites of pCAGGS/ES vector. mCerulean CDS was amplified by PCR using mCerulean-N1 vector as the template (Koushik et al., 2006)(a gift from Dr. Steven Vogel, Addgene #27795), and mPI31 CDS was cloned from a mouse cDNA library. The mCerulean-mPI31 cassette was inserted between the EcoRI/NheI sites of pCAGGS/ES vector.

All the constructs were validated by Sanger sequencing (Genewiz).

Generation of polyclonal antibody against *Drosophila* PI31

GST-PI31 was expressed in BL21 Star (DE3) *E.coli* cells(Thermo Fisher Scientific, #C601003), and purified using Glutathione Sepharose 4B beads (GE Healthcare, #17-0756-01). The purified protein was injected into rabbits and the antisera were collected (Cocalico).

Generation of MARCM clones

PI31$^{-/-}$ mutant clones were made using the mosaic analysis with a repressible cell marker (MARCM) system(Wu and Luo, 2006). The fly genotype is: *yw, hsp70-FLP*^{1}*; FRT42D, tubP-GAL80/FRT42D, PI31*$^{\Delta}$*; UAS- IVS-myr::GFP/D42-GAL4*. The eggs were laid on fly food at 25°C. The 0-6-hour embryos were heat-shocked at 37°C for 30mins followed by recovery at 25 °C for 30mins, and then heat-shocked again at 37°C for 45mins. The

wandering 3rd-instar larvae with the appropriate genotype were dissected and proceeded for immunostaining.

Generation of HA-PI31$^{Knock\text{-}in}$ fly

The off-target effect of gRNAs that are close to the 5′ end of the PI31 CDS was assessed by CRISPR target finder (http://tools.flycrispr.molbio.wisc.edu/targetFinder/) (Gratz et al., 2014) and E-CRISPR (www.e-crisp.org/E-CRISP/)(Heigwer et al., 2014). The selected sequence (AGTCGACCCACTTTCCATTG, on the "-" strand) was cloned into pCFD3-dU6:3gRNA vector (Port et al., 2014). A ssODN, which serves as the donor template for HDR-mediated recombination, was designed with ~50nt homology arm on each side, and synthesized (IDT). The full sequence of the ssODN is, CTTGTACAGCAGATCCCAACCGTAAAAGAAATCGCCCGTCTTGGCAGTCGACCCACTTTCGCCACCGCCGCTAGCATAGTCGGGCACATCATATGGGTACATTGCGGCCACCGATAATCCTTTACAAAATCTGGGTGGGAGTAAACAGAACGAATGGAAC. The pCFD3-dU6:3-PI31 gRNA construct (final concentration 150ng/µl) and the donor template ssODN (final concentration 200ng/µl) were mixed together and injected into the *y, sc, v; +/+; nos-Cas9*^{attP2} fly (Ren et al., 2013). Knock-in flies were initially identified by PCR and then confirmed by Sanger sequencing (Genewiz).

Immunofluorescence

Wandering 3rd-instar larvae were pinned on a silicone petri dish, and dissected in HL3 saline. The fillet preparations were fixed in 4% paraformaldehyde/PBS for 20mins. After washing with PBS/0.1% Triton X-100 (PBST), the fillets were blocked in 5% NGS/0.2% BSA/PBST, followed by incubation with primary antibodies overnight at 4°C. After washing for 3 times with 0.2%BSA/PBST, the secondary antibodies were applied at room temperature for 3 hours. The fillets were washed 4 times and proceeded for mounting and examination on a confocal microscope (LSM780, Zeiss). The following antibodies were used: chicken anti-mCherry (1:500, Novus, #NBP2-25158), rat anti-HA (1:100, clone 3F10, Sigma-Aldrich, #11867423001), mouse anti-ubiquitin conjugates (1:500, clone FK2, Enzo, #PW8810), mouse anti-Brp (1:300, clone nc82, Developmental Studies Hybridoma Bank, #nc82), chicken anti-GFP (1:1000, Aves Labs, #GFP-1020), rabbit anti-GluRIIC(Marrus et al., 2004) (1:1000, kindly provided by Dr. Aaron DiAntonio, Washington University in St. Louis), goat anti-rat-Alexa 488(1:500, Jackson ImmunoResearch, #112-545-167), goat anti-mouse-Alexa 488 plus (1:500, Thermo Fisher Scientific, #A32723), goat anti-chicken Alexa 488(1:500, Jackson ImmunoResearch, # 103-545-155), goat anti-chicken-Cy3(1:500, Jackson ImmunoResearch, #103-165-155), goat anti-mouse-Alexa 568(1:500, Thermo Fisher Scientific, #A11031), goat anti-HRP-Cy3(1:3000, Jackson ImmunoResearch, #123-165-021), goat anti-rabbit-Alexa 633(1:500, Thermo Fisher Scientific, #A21071), and goat anti-HRP-Alexa 647(1:300, Jackson ImmunoResearch, #123-605-021). Quantification of puncta number and intensity of Poly-Ub proteins was done with Fiji software(Schindelin et al., 2012), and Fiji and Imaris (Bitplane) softwares were used for quantification of numbers and volume of Brp puncta.

Co-Immunoprecipitation (Co-IP)

For the Co-IP experiments shown in Figure 2 and 3A, *tubP-GAL4, tubP-GAL80^{ts}* flies were crossed with *UAS-HA-PI31* or *yw* (as control) flies and raised at 25°C. The 0-3-day-old F1 progenies were collected and moved to 29°C for 6 days. Three-hundred male flies were collected and homogenized in 1.5ml buffer A [50mM Tris-HCl (pH7.5), 137mM NaCl, 0.25% NP-40, protease inhibitor cocktail (Roche, #11873580001) and phosphatase inhibitor cocktail(Roche, #04906837001)] . After centrifuged at 20000g for 15mins and filtered through a low-protein binding 0.45µm PVDF membrane syringe filter (Millipore, #SLHVX13NL), the extracts were incubated with 30µl mouse anti-HA agarose beads (clone HA-7, Sigma-Aldrich, #A2095) at 4°C for 3 hours. After six washes in buffer A and two additional washes in buffer A without NP-40 and protease and phosphatase inhibitors, the beads were eluted in 30µl 0.1M glycine (pH2.5) at room temperature for 10mins. The eluted proteins were taken either for mass spectrometry (MS) analysis (Figure 2) or for Western Blot (Figure 3A).

For the Co-IP experiment shown in Figure 3B, 150 3-day old male *HA-PI31$^{Knock\text{-}in}$* flies and *yw* flies (as control) were collected separately and homogenized in 1ml buffer A with 50U/ml DNase I (Thermo Fisher Scientific, #18047019). After centrifuged at 20000g for 15mins, sonicated briefly to break genomic DNAs, and filtered through a 0.45µm syringe filter, the extracts were incubated with 30µl mouse anti-HA magnetic beads (Thermo Fisher Scientific, #88836) at 4°C for 3 hours. After five washes in buffer A and two additional washes in buffer A without NP-40 and protease and phosphatase inhibitors, the beads were eluted in 30µl 500µg/ml HA peptide (Thermo Fisher Scientific, #26184) at 37°C for 30mins. The eluted proteins were analyzed by Western blot.

For the Co-IP experiments shown in Figure 3C, 3E, 4B and 5A, and Figure S4A and S4B, 10cm-plate cultures of indicated cell lines were transfected/infected with indicated constructs using TransIT-Insect transfection reagent (Mirus, #MIR6100) for S2 cells, Lipofectamine 2000 transfection reagent (Thermo Fisher Scientific, #11668-019) for HEK293 cells and lentivirus for MEFs, respectively. After 48 hours for the transfected cells or 7 days for the infected MEFs, the cell cultures were rinsed in cold PBS, collected, and resuspended in 0.6ml buffer A. Lysis was facilitated by freeze/thaw for three times. After centrifugation at 20000g for 15mins and filtration through a 0.45µm syringe filter, the extracts were incubated with 30µl mouse anti-HA agarose beads (clone HA-7, Sigma-Aldrich, #A2095), or 30µl mouse anti-FLAG magnetic beads (clone M2, Sigma-Aldrich, #M8823), or 30µl GFP-Trap agarose beads (Chromotek, gta-20) at 4°C for 3 hours. After six washes in buffer A, the beads were eluted in 30µl 1.5XSDS-PAGE sample buffer, boiled at 95°C for 5mins and analyzed by Western blot.

For the Co-IP experiment shown in Figure 4A, 10-cm plate cultures of S2 cells were transected with 15µg pAc5.1A-FLAG-dDYNLL1 or pAc5.1A empty vector (as control) constructs using TransIT-Insect transfection reagent. After 48 hours, the cells were rinsed, collected and resuspended in 600µl buffer A, and lysis was facilitated by freeze/thaw for three times. After centrifugation at 20000g for 15mins and filtration through a 0.45µm syringe filter, the extracts were incubated with 30µl mouse anti-FLAG magnetic beads (clone M2, Sigma-Aldrich, #M8823) at 4°C for 3 hours. After six washes

in buffer A and two additional washes in buffer A without NP-40 and protease and phosphatase inhibitors, the beads were eluted in 30µl 300 µg/ml 3XFLAG peptide (Sigma-Aldrich, #F4799) at 4°C for 45mins. The eluted proteins were run on a SDS-PAGE gel for ~1cm to remove the 3XFLAG peptide. Finally, the gel was cut for MS analysis. Biological triplicates of the Co-IP were used for quantification.

For the Co-IP experiment shown in Figure S4C, eight hundreds of 3-day-old male *HA-PI31*$^{Knock\text{-}in}$ flies and *yw* flies (as control) were collected separately and homogenized in 5ml buffer B [25mM HEPES (pH7.5), 100mM NaCl, 5mM MgCl2, 2mM ATP, 10% glycerol, 0.25% NP-40, protease inhibitor cocktail and phosphatase inhibitor cocktail] with 50U/ml DNase I (Thermo Fisher Scientific, #18047019). After centrifugation at 20000g for 15mins, lysates were sonicated briefly to break genomic DNA and filtered through a 0.45µm syringe filter, and then the extracts were incubated with 200µl mouse anti-HA magnetic beads (Thermo Fisher Scientific, #88836) at 4°C for 3 hours. After five washes in buffer B and two additional washes in buffer C [25mM HEPES (pH7.5), 150mM NaCl, 5mM $MgCl_2$, 2mM ATP, 10% glycerol], the beads were eluted by 200µl 500µg/ml HA peptide in buffer C at 37°C for 30mins. The eluted proteins were concentrated 5X with 10KDa-cutoff Amicon centrifugal filter unit (Millipore, #UFC501024), and analyzed by native gels and Western blot.

Mass spectrometry analysis

Glycine (0.1M, pH2.5) eluted samples (Figure 2) were dried in Speedvac concentrator (Thermo Fisher Scientific) and dissolved in 8M urea, 0.1M ammonium bicarbonate, and 10mM DTT. After reduction, cysteines were alkylated in 30mM iodoacetamide. The proteins were digested in less than 4M urea by endoproteinase LysC (Wako Chemicals) followed by digestion with Trypsin Gold (Promega) in less than 2M urea. FLAG-peptide eluted samples (Figure 4A) were cleaned up using SDS-PAGE, reduced (10mM DTT) and alkylated (30mM iodoacetamide), followed by digestion with a cocktail of LysC and Trypsin Gold. Digestions were halted by adding trifluoroacetic acid (TFA) and digests were desalted and analyzed by reversed phase nano-LC-MS/MS using either a Fusion Lumos or a Q-Exactive Plus (Thermo Fisher Scientific) both operated in high/high mode(Rappsilber et al., 2007).

Data were searched and quantified against a Uniprot's *Drosophila* database (21,945 sequences, March 2016) using Proteome Discoverer v1.4.0.288 (Thermo Fisher Scientific) combined with Mascot v2.5.1 (Matrix Science) and MaxQuant v1.6.0.13(Cox et al., 2014). Oxidation of methionine and protein N-terminal acetylation were allowed as variable modifications and all cysteines were treated as being carbamidomethylated. Peptide matches were filtered using a Percolator-calculated false discovery rate (FDR) of 1%(Kall et al., 2007). For the quantitative MaxQuant analysis, FDR thresholds for peptides and proteins were set at 2% and 1%, respectively.

Label Free Quantitation (LFQ) was used for the identification and quantitation of binding partners(Cox et al., 2014). Data were processed using Perseus v1.6.0.7(Tyanova et al., 2016). In short, reverse matches and common contaminations were disregarded, and protein signals in minimum 2 out of 3 replicates for at least one condition was

required. Data were validated by scatter plots, principal component analysis (PCA) and distributions of LFQ values, and found comparable. T-tests were performed and proteins were considered as interesting hits if showing a difference of more than 4-linear folds and a p-value of less than 0.01.

GST pull-down assays

BL21 Star (DE3) competent *E.coli* cells were transformed with pGEX-4T1-PI31, pGEX-4T1 empty vector or pET28a-FLAG-dDYNLL1. Single colonies were picked and cultured in 5ml LB, followed by an enlarged culture in 100ml LB. When OD_{600}≈0.4, IPTG was added to a final concentration of 0.3mM. After 4 hours, the bacteria were collected by centrifugation and rinsed by cold PBS. The bacteria were resuspended in 5ml cold PBS with protease inhibitor cocktail, lysed by sonication and centrifuged at 20000g for 15mins.

1ml pGEX-4T1 empty vector lysate or 1ml pGEX-4T1-PI31 lysate were incubated with 30µl Glutathione Sepharose 4B beads at 4°C for 3 hours. Then, the beads were washed with PBS for 3 times, followed by incubation with 1ml pET28a-FLAG-dDYNLL1 lysate at 4°C for 3 hours. The beads were washed in buffer A for five times and in 50 mM Tris-HCl (pH 8.0) once. Elution was done by incubation of the beads in 30µl GST elution buffer [50 mM Tris-HCl (pH 8.0) and 20mM reduced glutathione (Sigma-Aldrich, #G4251)] at room temperature for 20mins. The eluted proteins were analyzed by SDS-PAGE and Western blot. Ponceau S (Sigma-Aldrich, #P7170) staining was used to assess purity and amount of GST and GST-PI31. Anti-FLAG-HRP (1:1000, Sigma-Aldrich, #A8592) was used to evaluate amount of FLAG-dDYNLL1 bound to GST or GST-PI31.

***In vitro* reconstitution of the dDYNLL1-PI31-proteasome complex**

3ml lysate of BL21 Star (DE3) expressing pET28a-FLAG-dDYNLL1 was incubated with 100µl mouse anti-FLAG magnetic beads (clone M2, Sigma-Aldrich, #M8823) at 4°C for 3 hours. After washed with buffer A for four times, the beads were splitted equally into three tubes. Then, 5µg purified bovine 20S proteasome (UBPbio, #A1401), or 5µg GST+5µg purified bovine 20S proteasome, or 5µg GST-PI31+5µg purified bovine 20S proteasome were added to the three tubes, respectively, and incubated at 4°C for 3 hours. After four washes in buffer A, the beads were eluted in 35µl 300µg/ml 3XFLAG peptide at 4°C for 45mins.

Native gel assays

Protein complexes captured by anti-HA Co-IP using extracts of *yw* (as control) and *HA-PI31*$^{Knock\text{-}in}$ flies were eluted in buffer C with HA peptide under the native condition (see the "Co-IP" section for more details). The eluted proteins, as well as 15µg total lysates of *yw* and *HA-PI31*$^{Knock\text{-}in}$ flies (as inputs for the Co-IP experiment), were mixed with 2X native sample buffer (Bio-rad, #1610738), and loaded onto 3-8% Tris-acetate gels (Bio-rad, #3450131). Purified bovine 19S (UBPbio, #A1301), 20S (UBPbio, #A1401) and 26S (UBPbio, #A1201) proteasomes were also loaded onto the gels as standards to mark positions of different proteasome complexes. Electrophoresis was started with 50V for 1

hour in running buffer (90mM Tris, 90mM Boric Acid, 1mM EDTA, 2.5 mM MgCl2, 1mM ATP and 0.5mM DTT). After samples fully entered the gel, voltage was increased to 120V and ran 5 hours at 4°C. Then, proteins in the gels were transferred to PVDF membrane for Western Blot.

Western Blot Analysis

Proteins in SDS-PAGE gels or native gels were transferred onto 0.45µm Immobilon-P PVDF membranes (Millipore. #IPVH00010). The membranes were blocked with 5% non-fat milk in TBST [20mM Tris (pH7.5), 300mM NaCl, 0.1% Tween-20] at room temperature for 1 hour, followed by incubation with primary antibodies in 5% BSA/TBST at 4°C overnight. After washed for three times with TBST, the membranes were incubated with HRP-conjugated secondary antibodies at room temperature for 1.5 hours. The membranes were washed for four times with TBST, and detection was performed with ECL reagent (GE Healthcare, #RPN2134) or SuperSignal West Femto Maximum Sensitivity Substrate (Thermo Fisher Scientific, # 34096). The following antibodies were used for Western blot: rabbit anti-DYNLL1/2(1:3000, clone EP1660Y, Abcam, #ab51603), mouse anti-α7 (1:3000, clone MCP72, Enzo, # PW8110), mouse anti-Rpt3 (1:3000, clone TBP7-27, Enzo, # PW8765), rabbit anti-dPI31(1:5000), rat anti-HA-HRP(1:3000, clone 3F10, Roche, #12013819001), mouse anti-FLAG-HRP(1:1000, clone M2, Sigma-Aldrich, #A8592), mouse anti-GFP-HRP(1:1000, clone B2, Santa Cruz Biotechnology, #sc-9996-HRP), rabbit anti-GST-HRP(1:1000, Abcam, #ab3416), donkey anti-rabbit-HRP(1:5000, Jackson ImmunoResearch, #711-035-152), donkey anti-mouse-HRP(1:5000, Jackson ImmunoResearch, #715-035-150), goat anti-mouse Fc-HRP(1:3000, Thermo Fisher Scientific, #31437).

Live imaging

For analysis of proteasome transport in axons of *Drosophila* motor neurons, wandering 3rd-instar larvae of *R94G06-GAL4>Prosβ5-RFP* (as control) and *PI31$^{-/-}$, R94G06-GAL4>Prosβ5-RFP* were dissected in HL3 saline supplemented with 7mM L-glutamic acid, and flipped the inside out to expose motor neuron axons. The larval preparations were mounted on a microscope slide with coverslip bridges to avoid crash of tissues. Live imaging was done on a 60X silicone oil objective lens (NA1.3, Olympus) of inverted Olympus IX-70 microscope equipped with Evolve-512 EMCCD camera (Photometrics). Images were captured using a 500-ms exposure at 1.4 Hz, and each recording consisted of 100 frames in 70 seconds. Kymographs were generated and velocities of each proteasome particle were calculated using ImageJ with the "Multiple Kymograph" and "Walking Average" plugins. All particles were picked and tracked by the software. Seven wild-type larvae and twelve *PI31$^{-/-}$* larvae were analyzed.

For live imaging of α4-mCherry and mCerulean–PI31 in mouse DRG neuron cultures, DRGs were dissected from E13 mouse embryos (CD-1 IGS pregnant mouse, Charles River, #022) and dissociated to single cell suspension using Trypsin. Dissociated sensory neurons were transfected with pCAGGS/ES-α4-mCherry and pCAGGS/ES-mCerulean–mPI31 plasmids using the Neon transfection system (Thermo Fisher Scientific, MPK5000) at 1400 V, 20 ms, and 1 pulse. After transfection, $5X10^5$ neurons were centrifuged, resuspended in 9µl growth medium [Neurobasal medium (Thermo

Fisher Scientific, #21103049), B-27 (Thermo Fisher Scientific, #17504044), penicillin-streptomycin(Thermo Fisher Scientific, #15140122) with 12.5ng/ml mouse growth factor 2.5S (NGF, Alomone Labs, #N-100)] and transferred to 15µl growth medium as a hanging drop overnight to form cell aggregates. Aggregates were cut into four pieces, plated on Poly-D-Lysine (Sigma-Aldrich, #P6407)/Laminin (Sigma-Aldrich, #L2020)-coated 8-well µ-Slide (ibidi, # 80826) and cultured for additional 24-48 hours. Before imaging, culture medium was changed to Hibernate E low fluorescence media (BrainBits, #HELF) supplemented with B27 and NGF, in order to maintain cells in ambient CO_2 levels. Images were taken on a 60X silicone oil objective lens (NA1.3, Olympus) of inverted Olympus IX-70 microscope equipped with Evolve-512 EMCCD camera (Photometrics) and with a heating chamber at 37°C, at 0.5Hz for 1-3 minutes.

Acknowledgement
We thank Dr. Aaron DiAntonio for the GluRIIC antibody; Dr. Benjamin Eaton, the Bloomington *Drosophila* Stock Center, Vienna *Drosophila* Resource Center, FlyLight project team of Janelia Research Campus, and Flybase for *Drosophila* strains and relevant information. We are also grateful to Drs. Park Cho-Park, Simon Bullock, Michael Davidson, Didier Trono and Steven Vogel, and Addgene for plasmids. We thank Yetis Gultekin for his help in constructing the pLVX-EF1a-AcGFP-C1-mPI31 plasmid and generation of anti-PI31 antibody, and Drs. Alison North and Christina Pyrgaki for their help with live-imaging analysis. We also thank Drs. Michael Young, Sarit Larisch, Park Cho-Park, Mia Horowitz, Avi Levin, Sigi Benjamin-Hong, Dolors Ferres-Marco, Thomas Hsiao, Junko Shimazu, Wanhe Li, and Alana Persaud for valuable discussions. This work was supported by NIH grant RO1GM60124 and a generous gift from the Loewenberg Foundation to H.S.

References

Aguado, C., Sarkar, S., Korolchuk, V.I., Criado, O., Vernia, S., Boya, P., Sanz, P., de Cordoba, S.R., Knecht, E., and Rubinsztein, D.C. (2010). Laforin, the most common protein mutated in Lafora disease, regulates autophagy. Human molecular genetics *19*, 2867-2876.

Asano, S., Fukuda, Y., Beck, F., Aufderheide, A., Forster, F., Danev, R., and Baumeister, W. (2015). Proteasomes. A molecular census of 26S proteasomes in intact neurons. Science *347*, 439-442.

Bader, M., Benjamin, S., Wapinski, O.L., Smith, D.M., Goldberg, A.L., and Steller, H. (2011). A conserved F box regulatory complex controls proteasome activity in Drosophila. Cell *145*, 371-382.

Bai, C., Sen, P., Hofmann, K., Ma, L., Goebl, M., Harper, J.W., and Elledge, S.J. (1996). SKP1 connects cell cycle regulators to the ubiquitin proteolysis machinery through a novel motif, the F-box. Cell *86*, 263-274.

Balch, W.E., Morimoto, R.I., Dillin, A., and Kelly, J.W. (2008). Adapting proteostasis for disease intervention. Science *319*, 916-919.

Ballatore, C., Lee, V.M., and Trojanowski, J.Q. (2007). Tau-mediated neurodegeneration in Alzheimer's disease and related disorders. Nat Rev Neurosci *8*, 663-672.

Baumeister, W., Walz, J., Zuhl, F., and Seemuller, E. (1998). The proteasome: paradigm of a self-compartmentalizing protease. Cell *92*, 367-380.

Bingol, B., and Schuman, E.M. (2006). Activity-dependent dynamics and sequestration of proteasomes in dendritic spines. Nature *441*, 1144-1148.

Bingol, B., and Sheng, M. (2011). Deconstruction for reconstruction: the role of proteolysis in neural plasticity and disease. Neuron *69*, 22-32.

Bingol, B., Wang, C.F., Arnott, D., Cheng, D., Peng, J., and Sheng, M. (2010). Autophosphorylated CaMKIIalpha acts as a scaffold to recruit proteasomes to dendritic spines. Cell *140*, 567-578.

Callow, M.G., Tran, H., Phu, L., Lau, T., Lee, J., Sandoval, W.N., Liu, P.S., Bheddah, S., Tao, J., Lill, J.R.*, et al.* (2011). Ubiquitin Ligase RNF146 Regulates Tankyrase and Axin to Promote Wnt Signaling. PLOS ONE *6*, e22595.

Campbell, D.S., and Holt, C.E. (2001). Chemotropic responses of retinal growth cones mediated by rapid local protein synthesis and degradation. Neuron *32*, 1013-1026.

Chintapalli, V.R., Wang, J., and Dow, J.A. (2007). Using FlyAtlas to identify better Drosophila melanogaster models of human disease. Nature genetics *39*, 715-720.

Cho-Park, P.F., and Steller, H. (2013). Proteasome regulation by ADP-ribosylation. Cell *153*, 614-627.

Chu-Ping, M., Slaughter, C.A., and DeMartino, G.N. (1992). Purification and characterization of a protein inhibitor of the 20S proteasome (macropain). Biochim Biophys Acta *1119*, 303-311.

Coleman, M.P., and Perry, V.H. (2002). Axon pathology in neurological disease: a neglected therapeutic target. Trends Neurosci *25*, 532-537.

Collins, G.A., and Goldberg, A.L. (2017). The Logic of the 26S Proteasome. Cell *169*, 792-806.

Conedera, S., Apaydin, H., Li, Y., Yoshino, H., Ikeda, A., Matsushima, T., Funayama, M., Nishioka, K., and Hattori, N. (2016). FBXO7 mutations in Parkinson's disease and multiple system atrophy. Neurobiology of aging *40*, 192 e191-195.
Cox, J., Hein, M.Y., Luber, C.A., Paron, I., Nagaraj, N., and Mann, M. (2014). Accurate proteome-wide label-free quantification by delayed normalization and maximal peptide ratio extraction, termed MaxLFQ. Molecular & cellular proteomics : MCP *13*, 2513-2526.
Davis, L., Dou, P., DeWit, M., and Kater, S.B. (1992). Protein synthesis within neuronal growth cones. The Journal of neuroscience : the official journal of the Society for Neuroscience *12*, 4867-4877.
de Vrij, F.M., Fischer, D.F., van Leeuwen, F.W., and Hol, E.M. (2004). Protein quality control in Alzheimer's disease by the ubiquitin proteasome system. Prog Neurobiol *74*, 249-270.
Di Fonzo, A., Dekker, M.C., Montagna, P., Baruzzi, A., Yonova, E.H., Correia Guedes, L., Szczerbinska, A., Zhao, T., Dubbel-Hulsman, L.O., Wouters, C.H.*, et al.* (2009). FBXO7 mutations cause autosomal recessive, early-onset parkinsonian-pyramidal syndrome. Neurology *72*, 240-245.
DiAntonio, A., Haghighi, A.P., Portman, S.L., Lee, J.D., Amaranto, A.M., and Goodman, C.S. (2001). Ubiquitination-dependent mechanisms regulate synaptic growth and function. Nature *412*, 449-452.
Ding, M., Chao, D., Wang, G., and Shen, K. (2007). Spatial regulation of an E3 ubiquitin ligase directs selective synapse elimination. Science *317*, 947-951.
Djakovic, S.N., Marquez-Lona, E.M., Jakawich, S.K., Wright, R., Chu, C., Sutton, M.A., and Patrick, G.N. (2012). Phosphorylation of Rpt6 regulates synaptic strength in hippocampal neurons. The Journal of neuroscience : the official journal of the Society for Neuroscience *32*, 5126-5131.
Djakovic, S.N., Schwarz, L.A., Barylko, B., DeMartino, G.N., and Patrick, G.N. (2009). Regulation of the proteasome by neuronal activity and calcium/calmodulin-dependent protein kinase II. The Journal of biological chemistry *284*, 26655-26665.
Ehlers, M.D. (2003). Activity level controls postsynaptic composition and signaling via the ubiquitin-proteasome system. Nature neuroscience *6*, 231-242.
Erturk, A., Wang, Y., and Sheng, M. (2014). Local pruning of dendrites and spines by caspase-3-dependent and proteasome-limited mechanisms. The Journal of neuroscience : the official journal of the Society for Neuroscience *34*, 1672-1688.
Eskelinen, E.L., and Saftig, P. (2009). Autophagy: a lysosomal degradation pathway with a central role in health and disease. Biochimica et biophysica acta *1793*, 664-673.
Gendron, T.F., and Petrucelli, L. (2009). The role of tau in neurodegeneration. Molecular neurodegeneration *4*, 13.
Glickman, M.H., and Ciechanover, A. (2002). The ubiquitin-proteasome proteolytic pathway: destruction for the sake of construction. Physiological reviews *82*, 373-428.
Goldberg, A.L. (2003). Protein degradation and protection against misfolded or damaged proteins. Nature *426*, 895-899.

Gratz, S.J., Ukken, F.P., Rubinstein, C.D., Thiede, G., Donohue, L.K., Cummings, A.M., and O'Connor-Giles, K.M. (2014). Highly specific and efficient CRISPR/Cas9-catalyzed homology-directed repair in Drosophila. Genetics *196*, 961-971.
Hamilton, A.M., and Zito, K. (2013). Breaking it down: the ubiquitin proteasome system in neuronal morphogenesis. Neural Plast *2013*, 196848.
Hegde, A.N., Haynes, K.A., Bach, S.V., and Beckelman, B.C. (2014). Local ubiquitin-proteasome-mediated proteolysis and long-term synaptic plasticity. Frontiers in molecular neuroscience *7*, 96.
Heigwer, F., Kerr, G., and Boutros, M. (2014). E-CRISP: fast CRISPR target site identification. Nature methods *11*, 122-123.
Hirokawa, N., Niwa, S., and Tanaka, Y. (2010). Molecular motors in neurons: transport mechanisms and roles in brain function, development, and disease. Neuron *68*, 610-638.
Hoover, B.R., Reed, M.N., Su, J., Penrod, R.D., Kotilinek, L.A., Grant, M.K., Pitstick, R., Carlson, G.A., Lanier, L.M., Yuan, L.L.*, et al.* (2010). Tau mislocalization to dendritic spines mediates synaptic dysfunction independently of neurodegeneration. Neuron *68*, 1067-1081.
Hsu, M.T., Guo, C.L., Liou, A.Y., Chang, T.Y., Ng, M.C., Florea, B.I., Overkleeft, H.S., Wu, Y.L., Liao, J.C., and Cheng, P.L. (2015). Stage-Dependent Axon Transport of Proteasomes Contributes to Axon Development. Developmental cell *35*, 418-431.
Irvine, G.B., El-Agnaf, O.M., Shankar, G.M., and Walsh, D.M. (2008). Protein aggregation in the brain: the molecular basis for Alzheimer's and Parkinson's diseases. Mol Med *14*, 451-464.
Ittner, L.M., Ke, Y.D., Delerue, F., Bi, M., Gladbach, A., van Eersel, J., Wolfing, H., Chieng, B.C., Christie, M.J., Napier, I.A.*, et al.* (2010). Dendritic function of tau mediates amyloid-beta toxicity in Alzheimer's disease mouse models. Cell *142*, 387-397.
Johnson, J.O., Mandrioli, J., Benatar, M., Abramzon, Y., Van Deerlin, V.M., Trojanowski, J.Q., Gibbs, J.R., Brunetti, M., Gronka, S., Wuu, J.*, et al.* (2010). Exome sequencing reveals VCP mutations as a cause of familial ALS. Neuron *68*, 857-864.
Kall, L., Canterbury, J.D., Weston, J., Noble, W.S., and MacCoss, M.J. (2007). Semi-supervised learning for peptide identification from shotgun proteomics datasets. Nature methods *4*, 923-925.
Kenney, D.L., and Benarroch, E.E. (2015). The autophagy-lysosomal pathway: General concepts and clinical implications. Neurology *85*, 634-645.
Kipreos, E.T., and Pagano, M. (2000). The F-box protein family. Genome biology *1*, REVIEWS3002.
Kirk, R., Laman, H., Knowles, P.P., Murray-Rust, J., Lomonosov, M., Meziane el, K., and McDonald, N.Q. (2008). Structure of a conserved dimerization domain within the F-box protein Fbxo7 and the PI31 proteasome inhibitor. The Journal of biological chemistry *283*, 22325-22335.
Koppers, M., van Blitterswijk, M.M., Vlam, L., Rowicka, P.A., van Vught, P.W., Groen, E.J., Spliet, W.G., Engelen-Lee, J., Schelhaas, H.J., de Visser, M.*, et al.* (2012). VCP mutations in familial and sporadic amyotrophic lateral sclerosis. Neurobiology of aging *33*, 837 e837-813.

Koushik, S.V., Chen, H., Thaler, C., Puhl, H.L., 3rd, and Vogel, S.S. (2006). Cerulean, Venus, and VenusY67C FRET reference standards. Biophysical journal *91*, L99-L101.
Kreko-Pierce, T., and Eaton, B.A. (2017). The Drosophila LC8 homolog cut up specifies the axonal transport of proteasomes. Journal of cell science *130*, 3388-3398.
Kuo, C.T., Jan, L.Y., and Jan, Y.N. (2005). Dendrite-specific remodeling of Drosophila sensory neurons requires matrix metalloproteases, ubiquitin-proteasome, and ecdysone signaling. Proceedings of the National Academy of Sciences of the United States of America *102*, 15230-15235.
Lecker, S.H., Solomon, V., Mitch, W.E., and Goldberg, A.L. (1999). Muscle protein breakdown and the critical role of the ubiquitin-proteasome pathway in normal and disease states. The Journal of nutrition *129*, 227S-237S.
Lee, S.H., Choi, J.H., Lee, N., Lee, H.R., Kim, J.I., Yu, N.K., Choi, S.L., Lee, S.H., Kim, H., and Kaang, B.K. (2008). Synaptic protein degradation underlies destabilization of retrieved fear memory. Science *319*, 1253-1256.
Li, X., Thompson, D., Kumar, B., and DeMartino, G.N. (2014). Molecular and cellular roles of PI31 (PSMF1) protein in regulation of proteasome function. The Journal of biological chemistry *289*, 17392-17405.
Li, X.J., and Li, S. (2011). Proteasomal dysfunction in aging and Huntington disease. Neurobiology of disease *43*, 4-8.
Liu, C.W., Li, X., Thompson, D., Wooding, K., Chang, T.L., Tang, Z., Yu, H., Thomas, P.J., and DeMartino, G.N. (2006). ATP binding and ATP hydrolysis play distinct roles in the function of 26S proteasome. Molecular cell *24*, 39-50.
Marrus, S.B., Portman, S.L., Allen, M.J., Moffat, K.G., and DiAntonio, A. (2004). Differential localization of glutamate receptor subunits at the Drosophila neuromuscular junction. The Journal of neuroscience : the official journal of the Society for Neuroscience *24*, 1406-1415.
Martini-Stoica, H., Xu, Y., Ballabio, A., and Zheng, H. (2016). The Autophagy-Lysosomal Pathway in Neurodegeneration: A TFEB Perspective. Trends Neurosci *39*, 221-234.
McCutchen-Maloney, S.L., Matsuda, K., Shimbara, N., Binns, D.D., Tanaka, K., Slaughter, C.A., and DeMartino, G.N. (2000). cDNA cloning, expression, and functional characterization of PI31, a proline-rich inhibitor of the proteasome. The Journal of biological chemistry *275*, 18557-18565.
Mori, H., Kondo, J., and Ihara, Y. (1987). Ubiquitin is a component of paired helical filaments in Alzheimer's disease. Science *235*, 1641-1644.
Morimoto, R.I. (2008). Proteotoxic stress and inducible chaperone networks in neurodegenerative disease and aging. Genes & development *22*, 1427-1438.
Morishima-Kawashima, M., Hasegawa, M., Takio, K., Suzuki, M., Titani, K., and Ihara, Y. (1993). Ubiquitin is conjugated with amino-terminally processed tau in paired helical filaments. Neuron *10*, 1151-1160.
Oddo, S. (2008). The ubiquitin-proteasome system in Alzheimer's disease. J Cell Mol Med *12*, 363-373.
Olenych, S.G., Claxton, N.S., Ottenberg, G.K., and Davidson, M.W. (2007). The fluorescent protein color palette. Current protocols in cell biology *Chapter 21*, Unit 21 25.

Otero, M.G., Alloatti, M., Cromberg, L.E., Almenar-Queralt, A., Encalada, S.E., Pozo Devoto, V.M., Bruno, L., Goldstein, L.S., and Falzone, T.L. (2014). Fast axonal transport of the proteasome complex depends on membrane interaction and molecular motor function. J Cell Sci *127*, 1537-1549.
Paisan-Ruiz, C., Guevara, R., Federoff, M., Hanagasi, H., Sina, F., Elahi, E., Schneider, S.A., Schwingenschuh, P., Bajaj, N., Emre, M.*, et al.* (2010). Early-onset L-dopa-responsive parkinsonism with pyramidal signs due to ATP13A2, PLA2G6, FBXO7 and spatacsin mutations. Movement disorders : official journal of the Movement Disorder Society *25*, 1791-1800.
Pak, D.T., and Sheng, M. (2003). Targeted protein degradation and synapse remodeling by an inducible protein kinase. Science *302*, 1368-1373.
Pan, T., Kondo, S., Le, W., and Jankovic, J. (2008). The role of autophagy-lysosome pathway in neurodegeneration associated with Parkinson's disease. Brain : a journal of neurology *131*, 1969-1978.
Patrick, G.N. (2006). Synapse formation and plasticity: recent insights from the perspective of the ubiquitin proteasome system. Current opinion in neurobiology *16*, 90-94.
Perry, G., Friedman, R., Shaw, G., and Chau, V. (1987). Ubiquitin is detected in neurofibrillary tangles and senile plaque neurites of Alzheimer disease brains. Proceedings of the National Academy of Sciences of the United States of America *84*, 3033-3036.
Pfeiffer, B.D., Jenett, A., Hammonds, A.S., Ngo, T.T., Misra, S., Murphy, C., Scully, A., Carlson, J.W., Wan, K.H., Laverty, T.R.*, et al.* (2008). Tools for neuroanatomy and neurogenetics in Drosophila. Proceedings of the National Academy of Sciences of the United States of America *105*, 9715-9720.
Pfeiffer, B.D., Ngo, T.T., Hibbard, K.L., Murphy, C., Jenett, A., Truman, J.W., and Rubin, G.M. (2010). Refinement of tools for targeted gene expression in Drosophila. Genetics *186*, 735-755.
Port, F., Chen, H.M., Lee, T., and Bullock, S.L. (2014). Optimized CRISPR/Cas tools for efficient germline and somatic genome engineering in Drosophila. Proceedings of the National Academy of Sciences of the United States of America *111*, E2967-2976.
Qian, M.X., Pang, Y., Liu, C.H., Haratake, K., Du, B.Y., Ji, D.Y., Wang, G.F., Zhu, Q.Q., Song, W., Yu, Y.*, et al.* (2013). Acetylation-mediated proteasomal degradation of core histones during DNA repair and spermatogenesis. Cell *153*, 1012-1024.
Ramachandran, K.V., and Margolis, S.S. (2017). A mammalian nervous-system-specific plasma membrane proteasome complex that modulates neuronal function. Nature structural & molecular biology *24*, 419-430.
Rappsilber, J., Mann, M., and Ishihama, Y. (2007). Protocol for micro-purification, enrichment, pre-fractionation and storage of peptides for proteomics using StageTips. Nature protocols *2*, 1896-1906.
Ren, X., Sun, J., Housden, B.E., Hu, Y., Roesel, C., Lin, S., Liu, L.P., Yang, Z., Mao, D., Sun, L.*, et al.* (2013). Optimized gene editing technology for Drosophila melanogaster using germ line-specific Cas9. Proceedings of the National Academy of Sciences of the United States of America *110*, 19012-19017.
Ross, C.A., and Poirier, M.A. (2004). Protein aggregation and neurodegenerative disease. Nat Med *10 Suppl*, S10-17.

Rubinsztein, D.C. (2006). The roles of intracellular protein-degradation pathways in neurodegeneration. Nature *443*, 780-786.
Sandri, M. (2013). Protein breakdown in muscle wasting: role of autophagy-lysosome and ubiquitin-proteasome. The international journal of biochemistry & cell biology *45*, 2121-2129.
Schindelin, J., Arganda-Carreras, I., Frise, E., Kaynig, V., Longair, M., Pietzsch, T., Preibisch, S., Rueden, C., Saalfeld, S., Schmid, B.*, et al.* (2012). Fiji: an open-source platform for biological-image analysis. Nature methods *9*, 676-682.
Schliwa, M., and Woehlke, G. (2003). Molecular motors. Nature *422*, 759-765.
Sherva, R., Baldwin, C.T., Inzelberg, R., Vardarajan, B., Cupples, L.A., Lunetta, K., Bowirrat, A., Naj, A., Pericak-Vance, M., Friedland, R.P.*, et al.* (2011). Identification of novel candidate genes for Alzheimer's disease by autozygosity mapping using genome wide SNP data. Journal of Alzheimer's disease : JAD *23*, 349-359.
Skaar, J.R., Pagan, J.K., and Pagano, M. (2013). Mechanisms and function of substrate recruitment by F-box proteins. Nat Rev Mol Cell Biol *14*, 369-381.
Skowyra, D., Craig, K.L., Tyers, M., Elledge, S.J., and Harper, J.W. (1997). F-box proteins are receptors that recruit phosphorylated substrates to the SCF ubiquitin-ligase complex. Cell *91*, 209-219.
Speese, S.D., Trotta, N., Rodesch, C.K., Aravamudan, B., and Broadie, K. (2003). The ubiquitin proteasome system acutely regulates presynaptic protein turnover and synaptic efficacy. Current biology : CB *13*, 899-910.
Tai, H.C., and Schuman, E.M. (2008). Ubiquitin, the proteasome and protein degradation in neuronal function and dysfunction. Nature reviews Neuroscience *9*, 826-838.
Tyanova, S., Temu, T., Sinitcyn, P., Carlson, A., Hein, M.Y., Geiger, T., Mann, M., and Cox, J. (2016). The Perseus computational platform for comprehensive analysis of (prote)omics data. Nature methods *13*, 731-740.
Valakh, V., Naylor, S.A., Berns, D.S., and DiAntonio, A. (2012). A large-scale RNAi screen identifies functional classes of genes shaping synaptic development and maintenance. Developmental biology *366*, 163-171.
Vale, R.D. (2003). The molecular motor toolbox for intracellular transport. Cell *112*, 467-480.
Varshavsky, A. (2005). Regulated protein degradation. Trends in biochemical sciences *30*, 283-286.
Vingill, S., Brockelt, D., Lancelin, C., Tatenhorst, L., Dontcheva, G., Preisinger, C., Schwedhelm-Domeyer, N., Joseph, S., Mitkovski, M., Goebbels, S.*, et al.* (2016). Loss of FBXO7 (PARK15) results in reduced proteasome activity and models a parkinsonism-like phenotype in mice. The EMBO journal *35*, 2008-2025.
Wan, H.I., DiAntonio, A., Fetter, R.D., Bergstrom, K., Strauss, R., and Goodman, C.S. (2000). Highwire regulates synaptic growth in Drosophila. Neuron *26*, 313-329.
Watts, R.J., Hoopfer, E.D., and Luo, L. (2003). Axon pruning during Drosophila metamorphosis: evidence for local degeneration and requirement of the ubiquitin-proteasome system. Neuron *38*, 871-885.
Willeumier, K., Pulst, S.M., and Schweizer, F.E. (2006). Proteasome inhibition triggers activity-dependent increase in the size of the recycling vesicle pool in

cultured hippocampal neurons. The Journal of neuroscience : the official journal of the Society for Neuroscience *26*, 11333-11341.
Wu, J.S., and Luo, L. (2006). A protocol for mosaic analysis with a repressible cell marker (MARCM) in Drosophila. Nature protocols *1*, 2583-2589.
Yashiroda, H., Toda, Y., Otsu, S., Takagi, K., Mizushima, T., and Murata, S. (2015). N-terminal alpha7 deletion of the proteasome 20S core particle substitutes for yeast PI31 function. Molecular and cellular biology *35*, 141-152.
Yi, J.J., and Ehlers, M.D. (2005). Ubiquitin and protein turnover in synapse function. Neuron *47*, 629-632.
Yoshiyama, Y., Higuchi, M., Zhang, B., Huang, S.M., Iwata, N., Saido, T.C., Maeda, J., Suhara, T., Trojanowski, J.Q., and Lee, V.M. (2007). Synapse loss and microglial activation precede tangles in a P301S tauopathy mouse model. Neuron *53*, 337-351.
Yu, W., and Lu, B. (2012). Synapses and dendritic spines as pathogenic targets in Alzheimer's disease. Neural Plast *2012*, 247150.
Zaiss, D.M., Standera, S., Holzhutter, H., Kloetzel, P., and Sijts, A.J. (1999). The proteasome inhibitor PI31 competes with PA28 for binding to 20S proteasomes. FEBS Lett *457*, 333-338.
Zhao, Y., Hegde, A.N., and Martin, K.C. (2003). The ubiquitin proteasome system functions as an inhibitory constraint on synaptic strengthening. Current biology : CB *13*, 887-898.
Zhong, L., and Belote, J.M. (2007). The testis-specific proteasome subunit Prosalpha6T of D. melanogaster is required for individualization and nuclear maturation during spermatogenesis. Development *134*, 3517-3525.

Figure legends

Figure 1. PI31 is required for proteostasis and synaptic function in motor neurons.

(**A**) PI31 forms puncta in axons and at neuromuscular junctions (NMJs). The expression of UAS-HA-PI31 was driven by R94G06-GAL4, a specific motor neuron driver that only expresses in one motor neuron (MN1-IB) on each hemi-segment of the *Drosophila* larval ventral nerve cord, the axon of which targets Muscle 1(see Figure S1). Wandering 3rd-instar larvae were dissected, fixed and stained with an HA antibody (green), which labels HA-PI31, and a HRP antibody (red), which marks neuronal membranes. HA-PI31 forms puncta in axons and at NMJs of motor neurons.

(**B**) Loss of PI31 leads to accumulation of poly-ubiquitinated (Poly-Ub) protein in axons. Representative images for axons of wildtype and *PI31*$^{-/-}$ 3rd-instar larvae are shown. Poly-Ub proteins were stained with an anti-Ub conjugates antibody (clone FK2, green), and an anti-HRP antibody (red) was used to label neuronal membranes to visualize axons.

(**C**) Quantification of Poly-Ub protein puncta in axons. The Poly-Ub protein puncta from three different microscope views were counted for each larva. The numbers were added together and divided by the total area of axons. Five larvae were analyzed for each genotype. The bars represent mean+s.e.m. Unpaired two-tailed t-test, * $P<0.05$. Throughout the whole manuscript, blue bars represent wild-type or control conditions, whereas red bars represent *PI31*$^{-/-}$ conditions. *PI31*$^{-/-}$ larvae accumulate Poly-Ub protein puncta in axons.

(**D**) Loss of PI31 leads to accumulation of Poly-Ub proteins in NMJs. Representative images for Muscle 4 (M4) NMJs of wildtype and *PI31*$^{-/-}$ 3rd-instar larvae were shown. Poly-Ub proteins were stained with an anti-Ub conjugates antibody (clone FK2, green), and an anti-HRP antibody (red) was used to label neuronal membranes and indicate NMJ morphology.

(**E**) Quantification of immunofluorescence intensities of Poly-Ub proteins in M4 NMJs. Immuofluorecence intensities of Poly-Ub proteins were measured and normalized for the NMJ area. Twenty M4 NMJs from four larvae were analyzed for each genotype. The bars represent mean+s.e.m. Unpaired two-tailed t-test, *** $P<0.001$. *PI31*$^{-/-}$ larvae have increased Poly-Ub proteins in NMJs.

(**F**) High-magnification images for M4 NMJ boutons of wildtype and *PI31*$^{-/-}$ larvae immunostained with anti-Brp antibody (green), which labels presynaptic active zones, indicates that the number of synapses is reduced in *PI31*$^{-/-}$ NMJs. See Figure S2A for the overview of the M4 NMJs. See Figure S2B and S2C for the overview and high-magnification images of M6/7 NMJs.

(**G**) Quantification of Brp puncta at M4 and M6/7 (A2 segments) NMJs. Bars represent mean + standard deviation (s.d.). n=20 NMJs from four larvae for M4, and n=10 NMJs from six larvae for M6/7 at A2 segments. Unpaired two-tailed t-test, *** $P<0.001$. The result demonstrates that the number of synapses is significantly reduced in *PI31*$^{-/-}$ NMJs.

(**H**) Frequency distribution plot of Brp puncta volumes of M4 NMJs in wild-type and *PI31*$^{-/-}$ larvae. Volumes of each Brp punctum were measured. The x-axis indicates bin ranges, whereas the y-axis shows counts of Brp puncta, volumes of which fall into the indicated bin range. The measurement was done on the same images as (G). n=6853 Brp puncta from 20 NMJs for wild-type, and n= 3672 Brp puncta from 20 NMJs for *PI31*$^{-/-}$. The result reveals that the number of small synapses (volume<0.5μm^3) is severely

reduced, whereas big synapses (>0.5μm^3) are not affected in *PI31*$^{-/-}$ NMJs, suggesting that PI31 is important for maintenance of small synapses.
(**I**) Mosaic analysis with a repressible cell marker (MARCM) reveals that the reduction of synapse number in *PI31*$^{-/-}$ NMJs is a neuron-autonomous phenotype. The GFP-positive neuron (green) is *PI31*$^{-/-}$, whereas the GFP-negative neuron is *PI31*$^{+/-}$, which serves as an internal control. Brp antibody labels presynaptic active zones (red), and HRP antibody labels neuronal membranes (magenta). The control (*PI31*$^{+/-}$) and the *PI31*$^{-/-}$ M4 NMJs shown here were from the same larva. Shown here are high-magnification images, see Figure S2D for an overview of M4 NMJs.
(**J**) Quantification of Brp puncta at M4 NMJs of the *PI31*$^{-/-}$ MARCM clones. Bars represent mean + s.d. n=10 M4 NMJs from eight larvae for each genotype. Paired two-tailed t-test, *** *P<0.001*. The results demonstrate that the reduction of synapse number reflects a cell-autonomour requirement for PI31 in neurons.
(**K**)High-magnification images of MARCM M4 NMJs co-stained with a Brp antibody (red, a marker for presynaptic active zones) and a GluRIIC antibody (green, a marker for postsynaptic densities). The GFP-positive neuron (shown in a pseudo magenta color) is *PI31*$^{-/-}$, whereas the GFP-negative neuron is *PI31*$^{+/-}$. The white arrowheads point to regions that lost presynaptic active zones but still kept postsynaptic densities.
(**L**) Quantification of synapses that lost Brp but maintain GluRIIC. Bars represent mean + s.d. n=7 M4 NMJs from seven larvae for each genotype. Paired two-tailed t-test, ** *P<0.01*.

Figure 2. Identification of dDYNLL1/2 as binding partners of PI31 in *Drosophila*.
To study the interactome of PI31, we used *Tub-GAL4, Tub-GAL80*^{ts} to drive expression of *UAS-HA-PI31* transgene. Anti-HA Co-IP experiments were conducted with protein extracts of *Tub-GAL4, Tub-GAL80*^{ts} *>HA-PI31* files and *Tub-GAL4, Tub-GAL80*^{ts} flies (control). Eluted proteins were analyzed by label-free quantitative mass spectrometry. Volcano plot of the data is shown, based on biological triplicates of the Co-IP experiments. The x-axis represents $\log_2$ of fold differences, and the y-axis represents -$\log_{10}$ of *P*-value from *t-test*. The cutoff line for significance is *P*-value<0.01(-$\log_{10}$P >2) and fold difference>4 ($\log_2$fold difference >2 or <-2). PI31, dDYNLL1/2, 20S proteasome subunits and other statistically significant proteins are labeled in green, red, blue and pink, respectively; whereas ribosomal proteins and other statistically insignificant proteins are labeled in black and grey, respectively. The size of dots roughly indicates amount of a given protein detected by MS. dDYNLL1/2 are among the statistically most significant interactors of PI31, along with 20S proteasome subunits which were previously identified as PI31 interacting proteins.

Figure 3. PI31 directly interacts with dDYNLL1/2.
(**A**) The interaction between PI31 and dDYNLL1/2 was further confirmed by Co-IP and Western blot analysis. Anti-HA Co-IP experiments were performed with protein extracts of *Tub-GAL4, Tub-GAL80*^{ts}*>HA-PI31* flies and *Tub-GAL4, Tub-GAL80*^{ts} flies (control). Eluted proteins were analyzed by Western blot. A human DYNLL1 antibody that cross-reacts with dDYNLL1/2 was used to detect endogenous dDYNLL1/2(Kreko-Pierce and Eaton, 2017).

(**B**) PI31 can pull down dDYNLL1/2 at physiological levels of expression. To examine the interaction of PI31 and dDYNLL1/2 under conditions of endogenous expression levels, a HA-PI31$^{Kncok\text{-}in}$ fly strain was generated by insertion of a HA-tag into the N-terminus of PI31 genomic locus through CRISPR-HDR. The expression level of HA-PI31$^{Kncok\text{-}in}$ is comparable to the PI31 level in wild-type flies. Anti-HA Co-IP experiments were conducted and Western blot assay was used to detect dDYNLL1/2 and proteasomes. A human 20S proteasome subunit α7 antibody that cross-reacts with *Drosophila* α7 was used to detect proteasomes(Bader et al., 2011). This shows that PI31 interacts with dDYNLL1/2 and proteasomes at physiological expression levels.
(**C**) To further confirm the interaction between PI31 and dDYNLL1/Ctp, the reciprocal Co-IP was conducted using FLAG-dDYNLL1 as the bait. S2 cells expressing FLAG-dDYNLL1 and/or HA-PI31 were collected for anti-FLAG Co-IP experiments. Eluted proteins were analyzed with Western blot. The result indicates that FLAG-dDYNLL1 can pull down HA-PI31.
(**D**) GST-pull down assays were used to test for direct interaction between PI31 and dDYNLL1/Ctp. Recombinant GST-PI31 and FLAG-dDYNLL1 were generated in *E. coli.* GST-PI31 proteins were bound onto glutathione-agarose beads, and then FLAG-dDYNLL1 was applied to the beads. After washes, FLAG-dDYNLL1 bound to GST-PI31 was eluted and detected by Western blot using a FLAG antibody. Ponceau S that stains total proteins was used to assess amount and purity of recombinant GST and GST-PI31. The result demonstrates that purified GST-PI31 but not GST can pull down recombinant FLAG-dDYNLL1, indicating that PI31 and dDYNLL1/Ctp can bind directly to each other.
(**E**) The interaction between PI31 and DYNLL1/2 is conserved in mammals. Primary mouse embryonic fibroblasts (MEFs) were cultured and infected with lentivirus carrying the expression cassettes of GFP-mPI31 or GFP alone. Cells were collected and anti-GFP Co-IP experiments were conducted. Eluted proteins were analyzed by Western blot using a DYNLL1/2 antibody.

Figure 4. dDYNLL1/Ctp forms a protein complex with proteasomes
(**A**) Anti-FLAG-dDYNLL1 Co-IP and MS analysis reveal that dDYNLL1/Ctp forms a protein complex with proteasomes. Volcano plot of label-free quantitative MS analysis of anti-FLAG Co-IP experiments conducted with protein extract of S2 cells expressing FLAG-dDYNLL1 is shown. The x-axis represents log2 of fold changes, and the y-axis represents -log10 of *P*-value from t-test on biological triplicates of the Co-IP experiments. The cutoff line for significance is *P*-value<0.01($-\log_{10}P > 2$) and fold difference>4 ($\log_2$fold difference >2 or <-2). dDYNLL1/2, PI31, 20S proteasome subunits and other statistically significant proteins are labeled in red, green, blue and pink, respectively; whereas ribosomal proteins and other statistically insignificant proteins are labeled in black and grey, respectively. The size of dots roughly indicates amount of a given protein detected by MS. The result demonstrates that dDYNLL1/Ctp can pull down 20S proteasomes as well as PI31, suggesting they form a protein complex.
(**B**) Western blot analysis of anti-FLAG-dDYNLL1 Co-IP samples confirms the existence of dDYNLL1/Ctp-proteasome complexes. S2 cells expressing FLAG-dDYNLL1 were collected for anti-FLAG Co-IP experiments. Anti-α7, an antibody towards a 20S proteasome subunit was used to detect endogenous *Drosophila* α7. This

result is consistent with the MS data shown in (A) and confirms that dDYNLL1/Ctp forms a protein complex with proteasomes.

Figure 5. PI31 promotes formation of dDYNLL1/Ctp-proteasome complexes.
(**A**) PI31 promotes formation of dDYNLL1/Ctp-proteasome complexes in S2 cells. To test the role of PI31 on formation of dDYNLL1/Ctp-proteasome complexes, we expressed FLAG-dDYNLL1 with or without HA-PI31 in S2 cells, performed anti-FLAG Co-IP experiments and used Western blot against α7 subunit to detect proteasomes. The result indicates that PI31 can dramatically increase the amount of proteasomes bound to dDYNLL1/Ctp.
(**B**) PI31 promotes formation of dDYNLL1/Ctp-proteasome complexes *in vitro*. FLAG-dDYNLL1 was expressed in *E coli* and bound to anti-FLAG magnetic beads. Next, purified bovine 20S proteasomes were applied alone, or with GST or GST-PI31, which were expressed and purified from *E.coli.* GST-PI31, but not GST, largely increased the amount of proteasomes bound to dDYNLL1/Ctp *in vitro*. The left panel depicts a schematic model for the *in vitro* binding assay, and representative results from Western Blot analyses are shown on the right.

Figure 6. PI31 is required for axonal transport of proteasomes in motor neurons.
(**A**) Representative kymographs of Prosβ5-RFP motility in motor neurons of wild-type and *PI31*$^{-/-}$ 3rd-instar larvae. Prosβ5-RFP expression was driven by *R94G06-GAL4*, a motor neuron-specific driver (See Figure S1). The kymographs were generated from 70-second live imaging (100 frames). The x-axis represents distance, while the y-axis represents time. Stationary particles appear as vertical lines, whereas motile particles appear as diagonal lines on kymographs. The directions of anterograde and retrograde transport are indicated on top of the kymographs. The results show that loss of PI31 causes severely reduced motility of proteasomes in axons.
(**B**) Quantification of proteasome movement. The fractions of Prosβ5-RFP particles that moved in anterograde direction, retrograde direction or appeared stationary/moved randomly in axons of wild-type and *PI31*$^{-/-}$ motor neurons are shown. Bars represent mean + s.e.m. n=216 particles for wild-type, n=224 particles for *PI31*$^{-/-}$. Unpaired two-tailed t-test, ***$P<0.001$. In axons of *PI31*$^{-/-}$ motor neurons, both anterograde and retrograde movements of proteasome particles was drastically reduced, while the portion of stationary/randomly moving proteasome increased accordingly.
(**C**) Average velocities of moving Prosβ5-RFP particles in axons of wild-type and *PI31*$^{-/-}$ motor neurons. Bars represent mean + s.e.m. n=161 particles for wild-type, n=41 particles for PI31$^{-/-}$. Unpaired two-tailed t-test, ***$P<0.001$, ** $P<0.01$. The small number of proteasome particles in *PI31*$^{-/-}$ neurons had significantly reduced velocities.
(**D**) Representative images showing axons of cultured mouse DRG neurons expressing mCerulean-mPI31 (green) and α4-mCherry (red). mPI31 and proteasome particles extensively co-localized in axons.
(**E**) Kymographs indicating the motility of mCerulean-mPI31 (upper panel) and α4-mCherry (lower panel) particles from (D). The kymographs were generated from a 140-second live imaging experiment (70 frames). The overlap in motility tracks shows that mCerulean-mPI31 and proteasomes (labeled with α4-mCherry) move together in axons.

Figure 7. Model for PI31-mediated transport of proteasomes in axons.
Proteasomes can move rapidly along microtubules, allowing them to fulfill dynamic local demands for protein degradation in different cellular compartments(DiAntonio et al., 2001; Hegde et al., 2014; Hsu et al., 2015; Kreko-Pierce and Eaton, 2017; Watts et al., 2003; Zhao et al., 2003). PI31 binds directly to both proteasomes and dynein light chain LC8-type proteins (DYNLL1/2), which play a key role in microtubule-dependent transport(Bader et al., 2011; Cho-Park and Steller, 2013; Chu-Ping et al., 1992; Hsu et al., 2015; Kreko-Pierce and Eaton, 2017; Liu et al., 2018). Inactivation of PI31 severely reduces proteasome movement in *Drosophila* and leads to the accumulation of Poly-Ub aggregates in the periphery of neurons. This suggests that PI31 functions as a direct adaptor to couple proteasomes to microtubule-based motors. If this mechanism is impaired, insufficient numbers of proteasomes reach the synapse, causing failure to degrade synaptic proteins.

Supplementary figure legends

Figure S1. The expression pattern of *R94G06-GAL4* illustrated by using it to drive *UAS-mCD8-mCherry*.

(**A**) Brain and ventral nerve cord.
(**B**) A single axon in nerve.
(**C**) Neuromuscular junction (NMJ) at Muscle 1.
A Brp antibody (clone nc82, green) was used to visualize the synaptic neuropil regions. The results indicate that *R94G06-GAL4* is a specific driver for a subset of motor neurons (MN1-IB) targeting Muscle 1.

Figure S2. Synapse number at NMJs is reduced in *PI31* $^{-/-}$ larva.

(**A**) The overview images for M4 NMJs of wild-type and *PI31*$^{-/-}$ larvae immunostained with anti-Brp (green) and anti-HRP(magenta) antibodies, indicating that the number of synapses is reduced in *PI31* $^{-/-}$ larvae. Brp and HRP antibodies label presynaptic active zones and neuronal membranes, respectively. The higher-magnification images of the boxed area are shown in Figure 1F, and quantification of synapse number is shown in Figure 1G.
(**B-C**) Representative images of NMJs at M6/7, indicating that the number of synapses is reduced in *PI31* $^{-/-}$ larvae. Wild-type and *PI31*$^{-/-}$ 3rd-instar larvae were immunostained with anti-Brp (green) and anti-HRP (magenta) antibodies. (**B**) Overview of M6/7 NMJs. (**C**) High magnification of the boxed area in (B). See quantification of synapse number in Figure 1G.
(**D**) Analysis of *PI31*$^{-/-}$ MARCM clones reveals that the reduction of synapse number is a neuron-autonomous phenotype. The GFP-positive neuron is *PI31*$^{-/-}$, whereas the GFP-negative neuron is *PI31*$^{+/-}$ (control). The control (*PI31*$^{+/-}$) and the *PI31*$^{-/-}$ M4 NMJs shown here are from the same larva. The high-magnification images of the boxed regions are shown in Figure 1I, and quantification of synapse number is shown in Figure 1J.

Figure S3. dDYNLL1/2 are binding partners of PI31.

(**A**) Alignment of dDYNLL1/Ctp and dDYNLL2/Cdlc2. They differ in only one amino acid, which is highlighted by a pink box. The alignment was performed with Clustal Omega program on Uniprot server.
(**B**) The spectra of the unique peptides for dDYNLL1/Ctp and dDYNLL2/Cdlc2 that Co-IP with HA-PI31, indicating that both proteins interact with PI31. The unique peptides from both dDYNLL1/Ctp (peptide sequence: DIAAYIK, panel a) and dDYNLL2/Cdlc2 (peptide sequence: DIAAFIK, panel b) were identified in the anti-HA-PI31 Co-IP samples using nano liquid chromatography and high-resolution MS. Both unique peptides were matched with high confidence and with mass accuracy of better than 0.5ppm.

Figure S4. DYNLL1/2 are binding partners of PI31 in S2 cells and HEK293 cells.

(**A**) Western blot analysis of anti-HA Co-IP experiments using protein extracts of S2 cells expressing HA-PI31, indicating that PI31 interacts dDYNLL1/2 in S2 cells.
(**B**) Western blot analysis of anti-HA Co-IP experiments using protein extracts of HEK293 cells expressing HA-hPI31, indicating that the interaction between PI31 and DYNLL1/2 is conserved in human cells.

(**C**)Native gel analysis of PI31-bound complexes indicates that PI31 binds to both 20S and single-capped 26S proteasomes. HA-PI31$^{Knock\text{-}in}$ flies were collected, and anti-HA Co-IP experiments were conducted. The HA-PI31 and its interacting proteins were eluted by HA peptide under native conditions, and resolved on native gels. ATP is present during the Co-IP and native gel procedures. Anti-α7 and anti-Rpt3 antibodies that cross-react with respective *Drosophila* proteins were used for Western blot to visualize 20S(α7), 19S(Rpt3) and 26S(both α7 and Rpt3) proteasomes. The results demonstrate that PI31 can bind to both 20S and single-capped 26S proteasomes, and may involve in their transport.

Movie S1. A representative video of Pros**β**5-RFP particle movement in an axon of a wild-type larva (*w; +/+; R94G06-GAL4, UAS-Prosβ5-RFP/R94G06-GAL4, UAS-Prosβ5-RFP*). The video was acquired at 1.4Hz rate for 70 seconds (100 frames in total), and is shown in 10X of the original speed.

Movie S2. A representative video of Pros**β**5-RFP particle movement in an axon of a *PI31*$^{-/-}$ larva (*w; PI31*$^{\Delta}$*/ PI31*$^{\Delta}$*; R94G06-GAL4, UAS-Prosβ5-RFP/R94G06-GAL4, UAS-Prosβ5-RFP*). The video was acquired at 1.4Hz rate for 70 seconds (100 frames in total), and is shown in 10X of the original speed.

Movie S3. A representative video of mCerulean-mPI31 (green) and α4-mCherry (red) movement in axons of cultured mouse DRG neurons. The video was acquired at 0.5Hz rate for 140 seconds (70 frames in total), and is shown in 10X of the original speed.

Table S1. Inactivation of PI31 in neurons results in an eclosion defect.

Figure 1

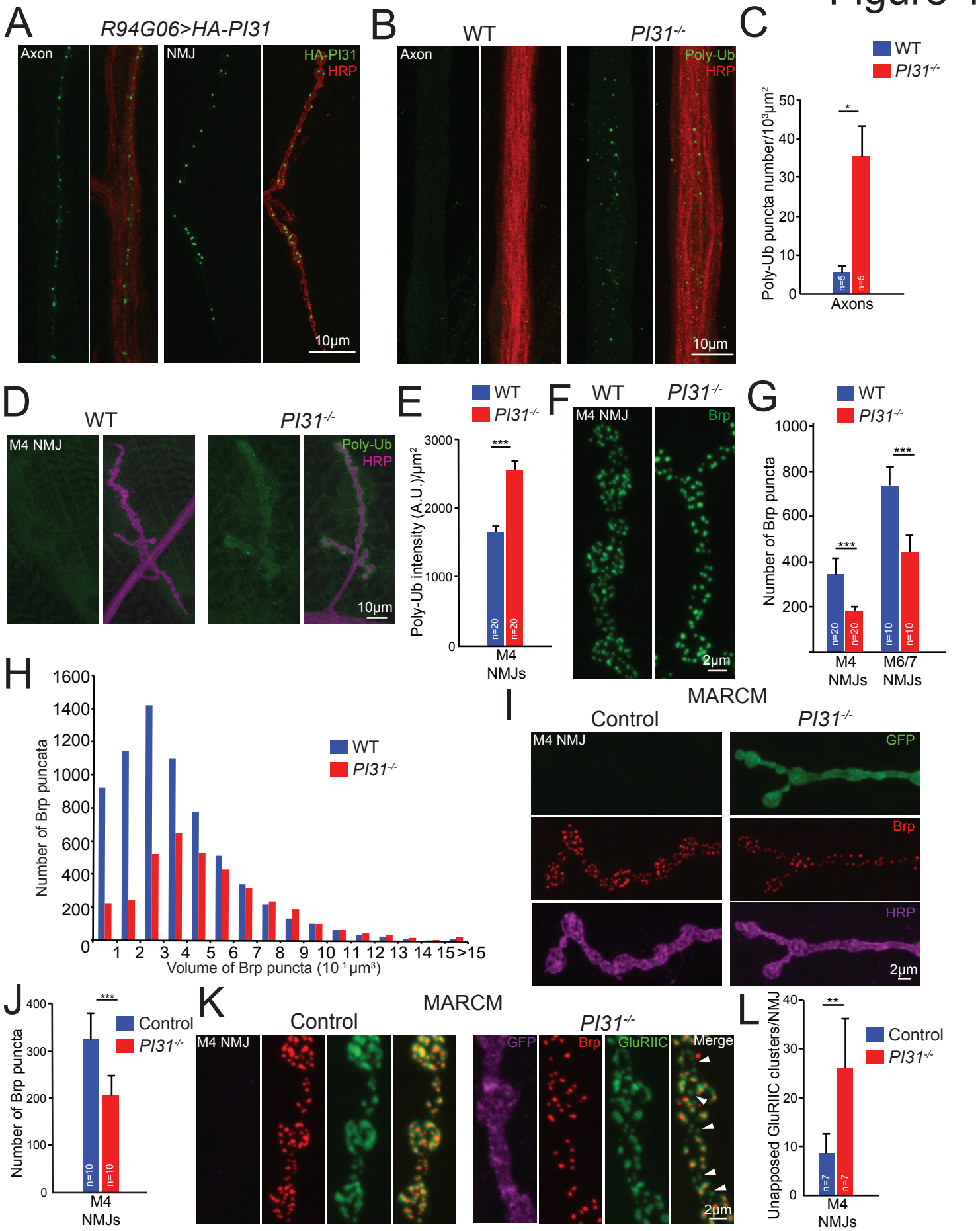
A
R94G06>HA-PI31
Axon
NMJ
HA-PI31
HRP
10µm
B
WT
PI31-/-
Axon
Poly-Ub
HRP
10µm
C
WT
PI31-/-
Poly-Ub puncta number/10³µm²
50
40
30
20
10
0
*
n=5
n=5
Axons
D
WT
PI31-/-
M4 NMJ
Poly-Ub
HRP
10µm
E
WT
PI31-/-
Poly-Ub intensity (A.U.)/µm²
3000
2000
1000
0
***
n=20
n=20
M4
NMJs
F
WT
PI31-/-
M4 NMJ
Brp
2µm
G
WT
PI31-/-
Number of Brp puncta
1000
800
600
400
200
***
***
n=20
n=20
n=10
n=10
M4
NMJs
M6/7
NMJs
H
Number of Brp puncata
1600
1400
1200
1000
800
600
400
200
0
WT
PI31-/-
1 2 3 4 5 6 7 8 9 10 11 12 13 14 15 >15
Volume of Brp puncta (10⁻¹ µm³)
I
MARCM
Control
PI31-/-
M4 NMJ
GFP
Brp
HRP
2µm
J
Number of Brp puncta
400
300
200
100
0
***
Control
PI31-/-
n=10
n=10
M4
NMJs
K
MARCM
Control
PI31-/-
M4 NMJ
GFP
Brp
GluRIIC
Merge
2µm
L
Unapposed GluRIIC clusters/NMJ
40
30
20
10
0
**
Control
PI31-/-
n=7
n=7
M4
NMJs

Figure 2

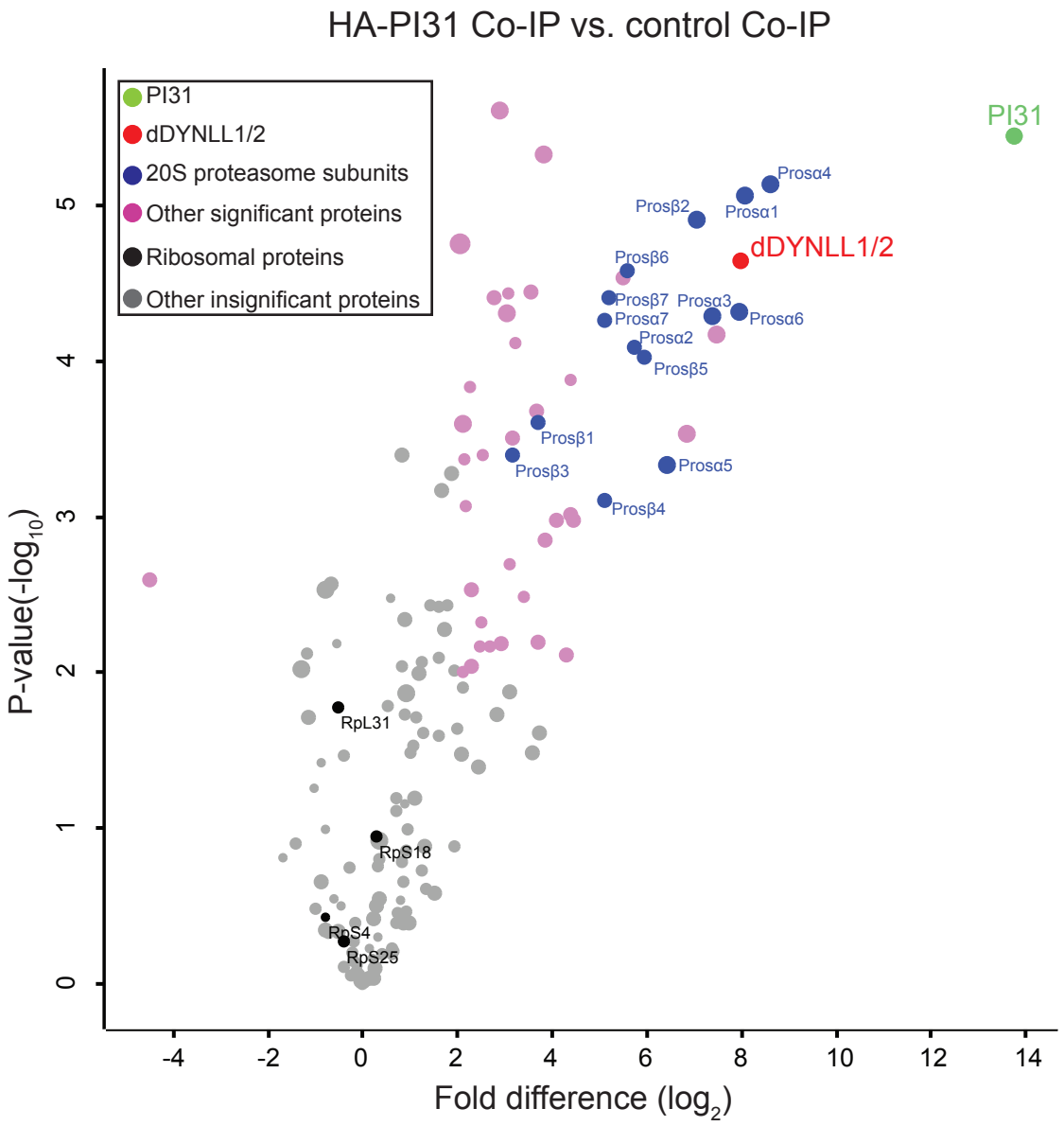
HA-PI31 Co-IP vs. control Co-IP
PI31
dDYNLL1/2
20S proteasome subunits
Other significant proteins
Ribosomal proteins
Other insignificant proteins
PI31
Prosα4
Prosβ2
Prosα1
dDYNLL1/2
Prosβ6
Prosβ7
Prosα3
Prosα6
Prosα7
Prosα2
Prosβ5
Prosβ1
Prosβ3
Prosα5
Prosβ4
RpL31
RpS18
RpS4
RpS25
P-value(-log10)
Fold difference (log2)
-4
-2
0
2
4
6
8
10
12
14
0
1
2
3
4
5

Figure 3

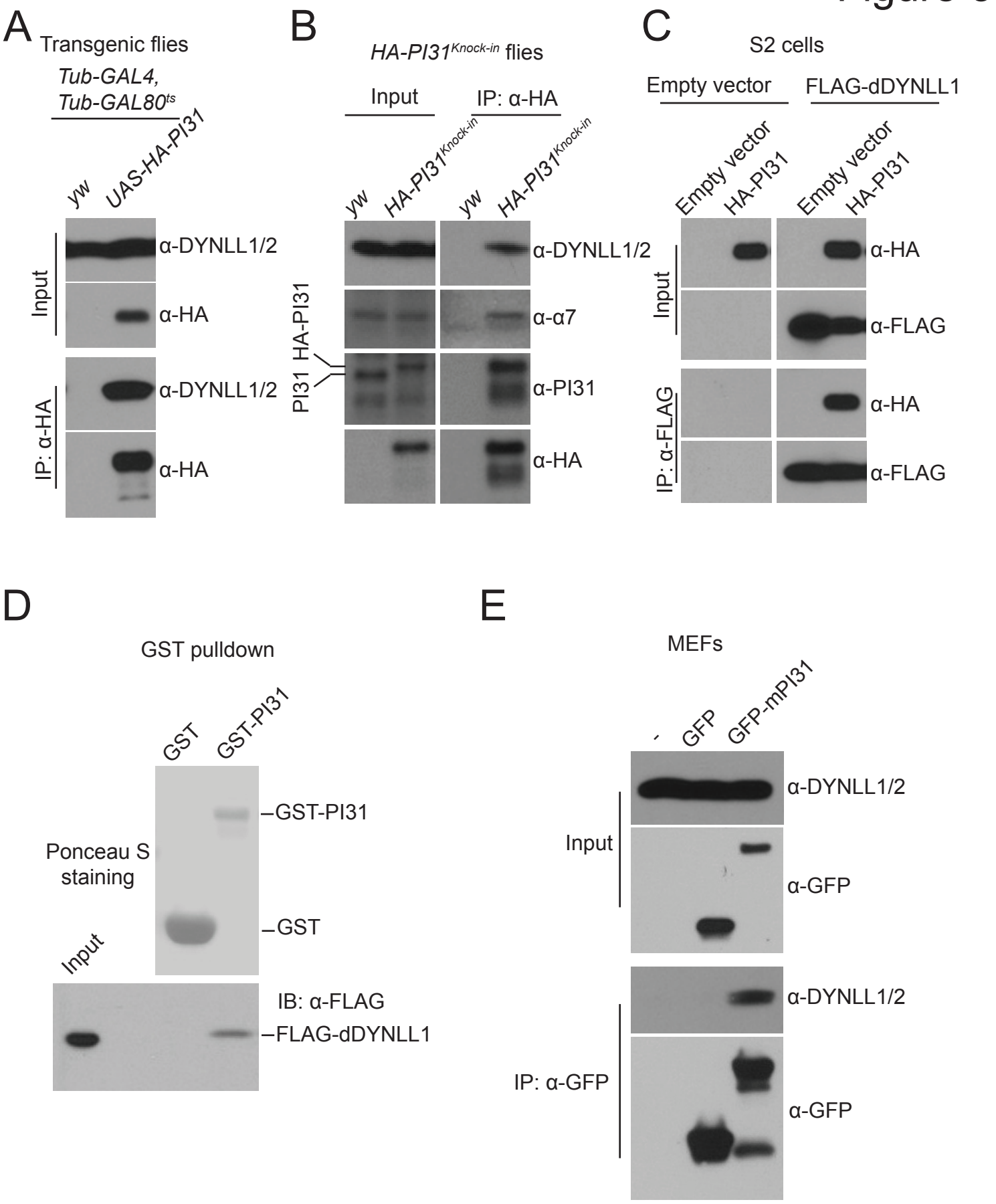
A
Transgenic flies
Tub-GAL4,
Tub-GAL80ts
yw
UAS-HA-PI31
Input
IP: α-HA
α-DYNLL1/2
α-HA
α-DYNLL1/2
α-HA
B
HA-PI31Knock-in flies
Input
IP: α-HA
yw
HA-PI31Knock-in
yw
HA-PI31Knock-in
α-DYNLL1/2
α-α7
HA-PI31
PI31
α-PI31
α-HA
C
S2 cells
Empty vector
FLAG-dDYNLL1
Empty vector
HA-PI31
Empty vector
HA-PI31
Input
IP: α-FLAG
α-HA
α-FLAG
α-HA
α-FLAG
D
GST pulldown
GST
GST-PI31
Ponceau S
staining
GST-PI31
GST
Input
IB: α-FLAG
FLAG-dDYNLL1
E
MEFs
-
GFP
GFP-mPI31
Input
IP: α-GFP
α-DYNLL1/2
α-GFP
α-DYNLL1/2
α-GFP

Figure 4

A

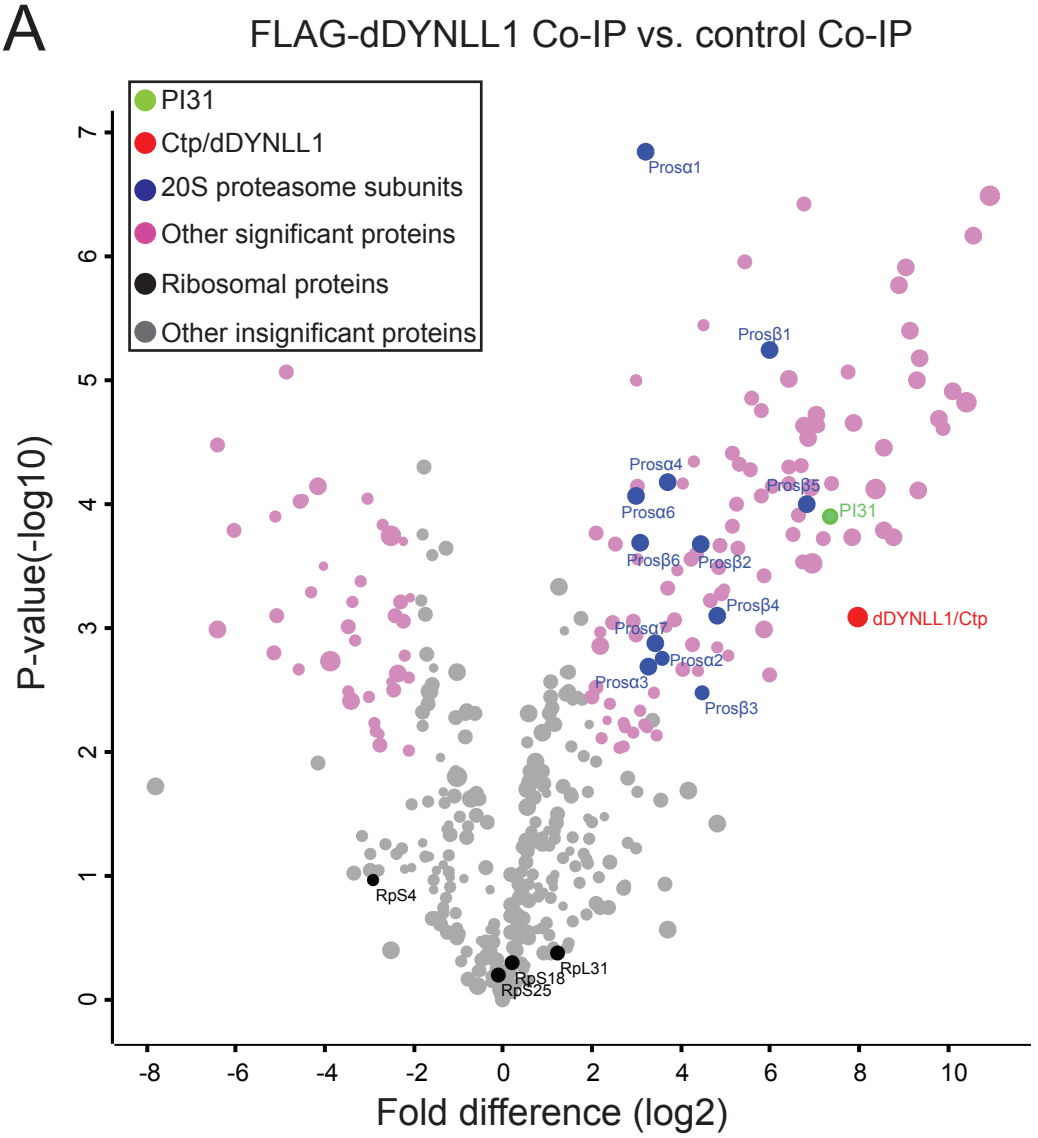
FLAG-dDYNLL1 Co-IP vs. control Co-IP
PI31
Ctp/dDYNLL1
20S proteasome subunits
Other significant proteins
Ribosomal proteins
Other insignificant proteins
Prosα1
Prosβ1
Prosα4
Prosβ5
PI31
Prosα6
Prosβ6
Prosβ2
Prosβ4
dDYNLL1/Ctp
Prosα7
Prosα2
Prosα3
Prosβ3
RpS4
RpS18
RpS25
RpL31
P-value(-log10)
Fold difference (log2)

B

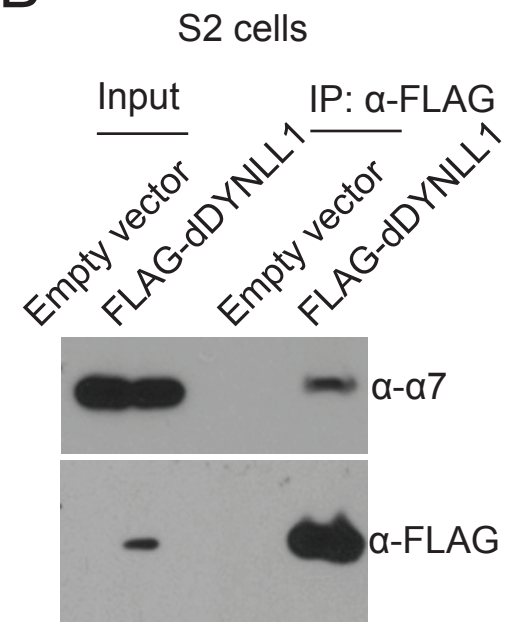
S2 cells
Input
IP: α-FLAG
Empty vector
FLAG-dDYNLL1
Empty vector
FLAG-dDYNLL1
α-α7
α-FLAG

Figure 5

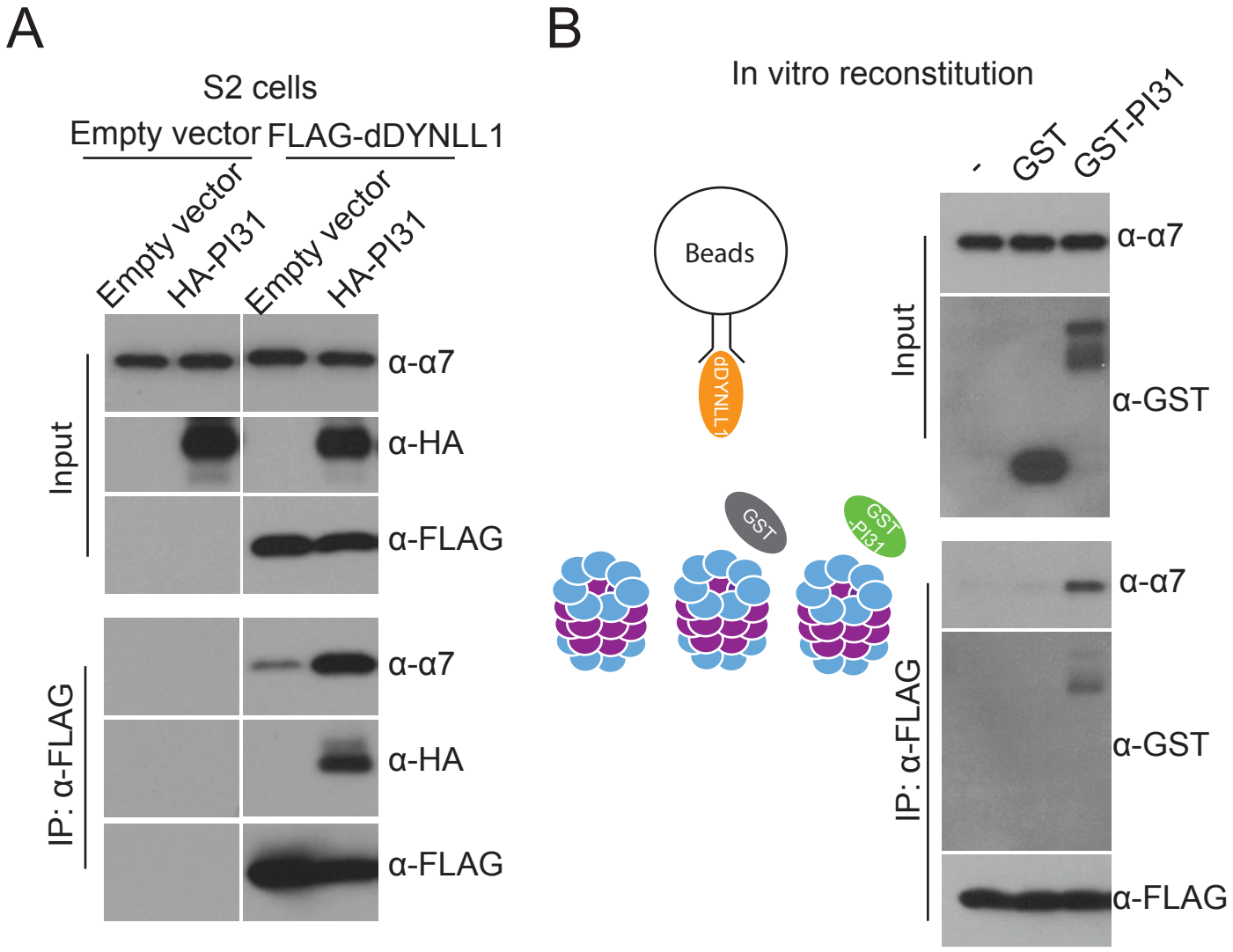
A
S2 cells
Empty vector
FLAG-dDYNLL1
Empty vector
HA-PI31
Empty vector
HA-PI31
Input
α-α7
α-HA
α-FLAG
IP: α-FLAG
α-α7
α-HA
α-FLAG
B
In vitro reconstitution
-
GST
GST-PI31
Beads
dDYNLL1
GST
GST-PI31
Input
α-α7
α-GST
IP: α-FLAG
α-α7
α-GST
α-FLAG

Figure 6

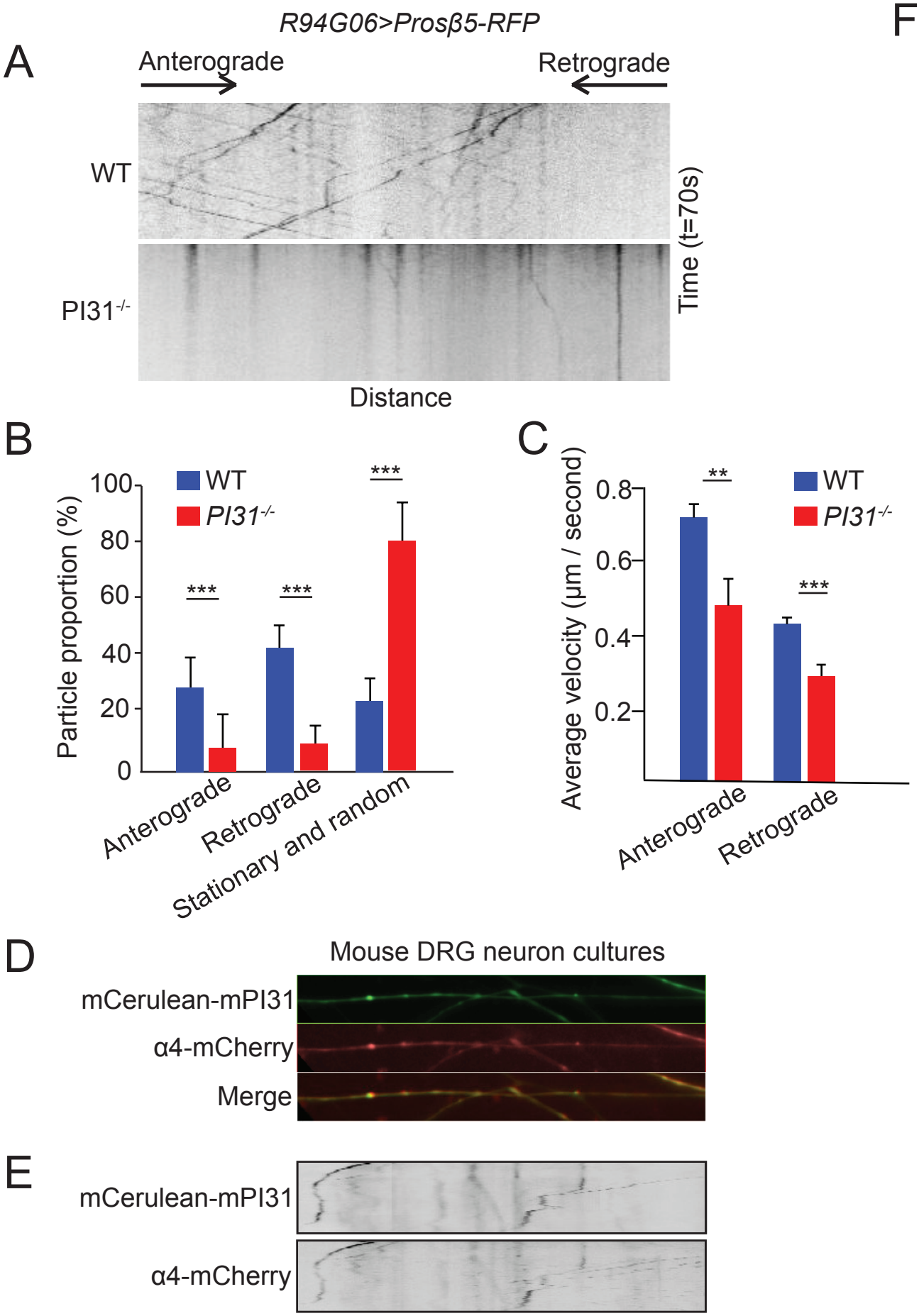
A
R94G06>Prosβ5-RFP
Anterograde
Retrograde
WT
PI31-/-
Time (t=70s)
Distance
B
Particle proportion (%)
100
80
60
40
20
0
WT
PI31-/-
***
***
***
Anterograde
Retrograde
Stationary and random
C
Average velocity (µm / second)
0.8
0.6
0.4
0.2
**
***
WT
PI31-/-
Anterograde
Retrograde
D
Mouse DRG neuron cultures
mCerulean-mPI31
α4-mCherry
Merge
E
mCerulean-mPI31
α4-mCherry

Figure 7

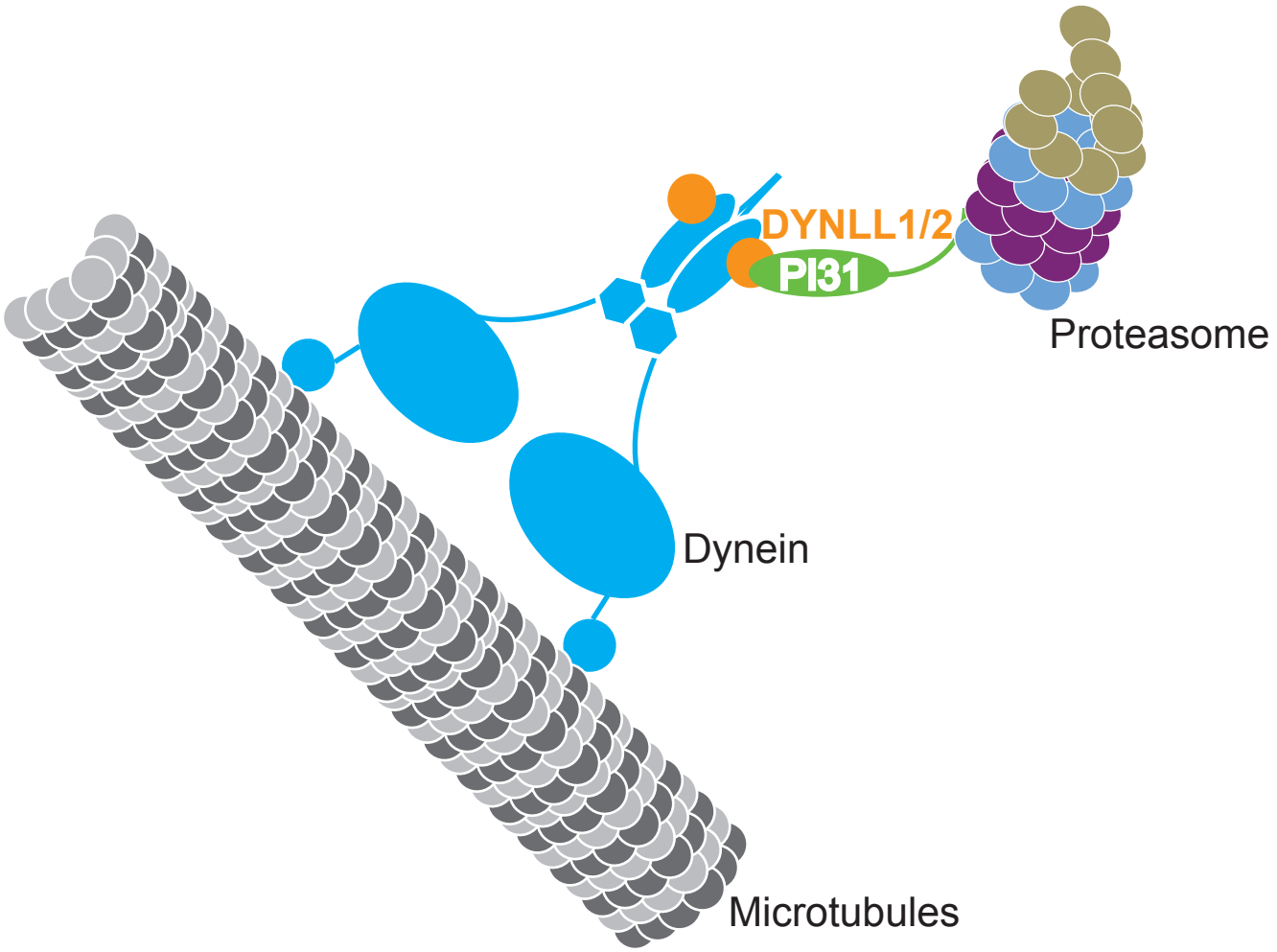

Figure S1

R94G06-GAL4>UAS-mCD8-mCherry

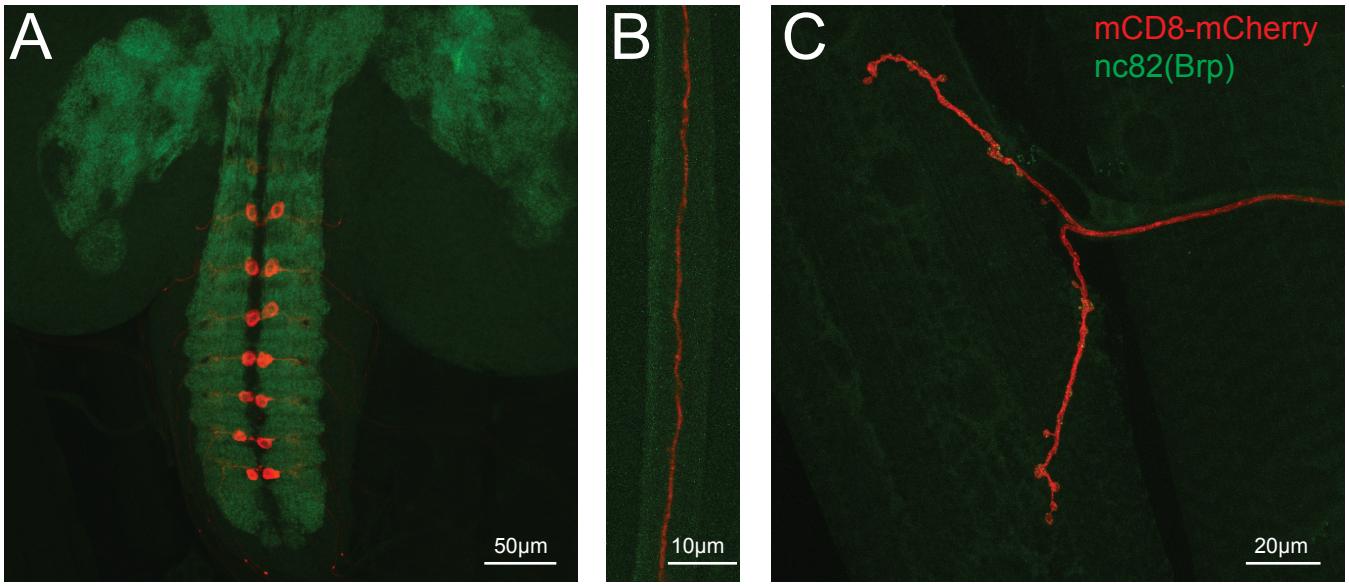

Figure S2

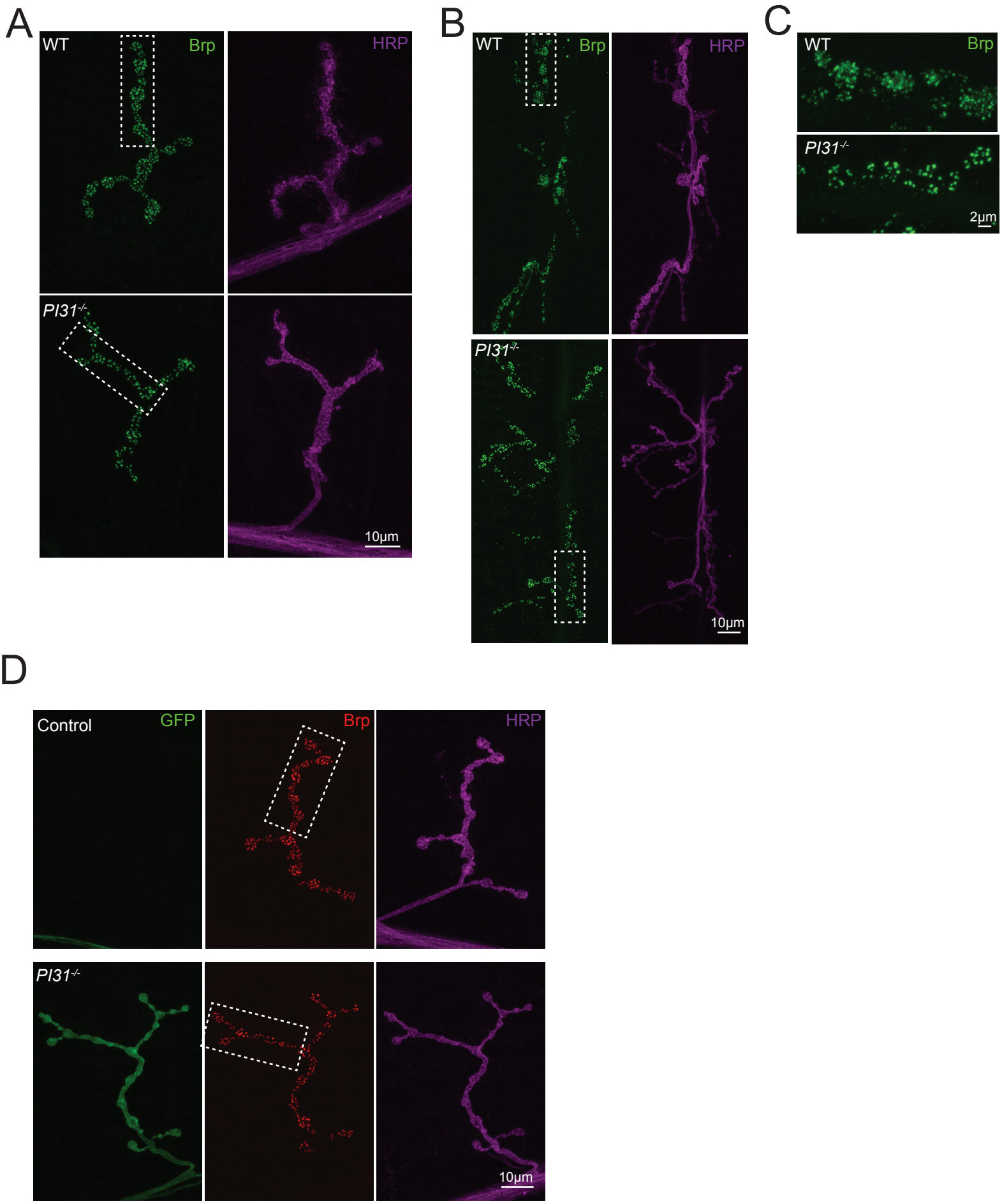
A
WT
Brp
HRP
PI31-/-
10μm
B
WT
Brp
HRP
PI31-/-
10μm
C
WT
Brp
PI31-/-
2μm
D
Control
GFP
Brp
HRP
PI31-/-
10μm

Figure S3

A

```
dDYNLL1/Ctp    MSDRKAVIKNADMSEEMQQDAVDCATQALEKYNIEKDIAAYIKKEFDKKYNPTWHCIVGRNFGSYVTHETRHFIYFYLGQVAILLFKSG
dDYNLL2/Cdlc2  MSDRKAVIKNADMSEEMQQDAVDCATQALEKYNIEKDIAAFIKKEFDKKYNPTWHCIVGRNFGSYVTHETRHFIYFYLGQVAILLFKSG
               ****************************************:***************************************************
```

B

a

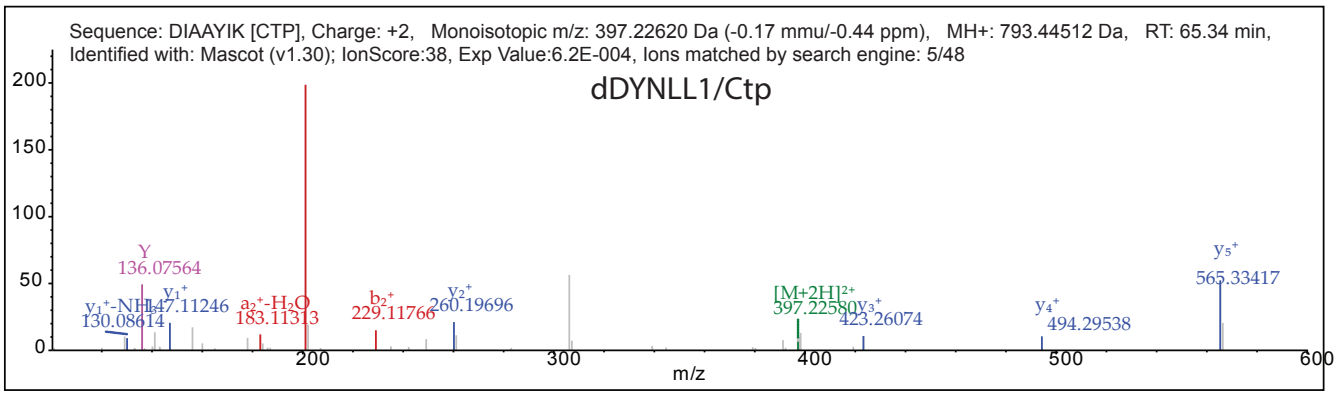

b

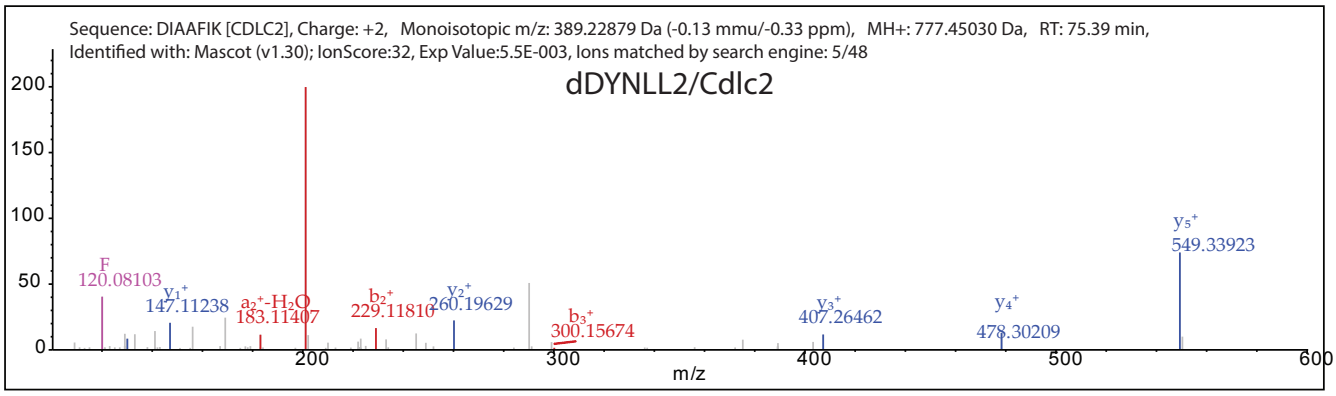

Figure S4

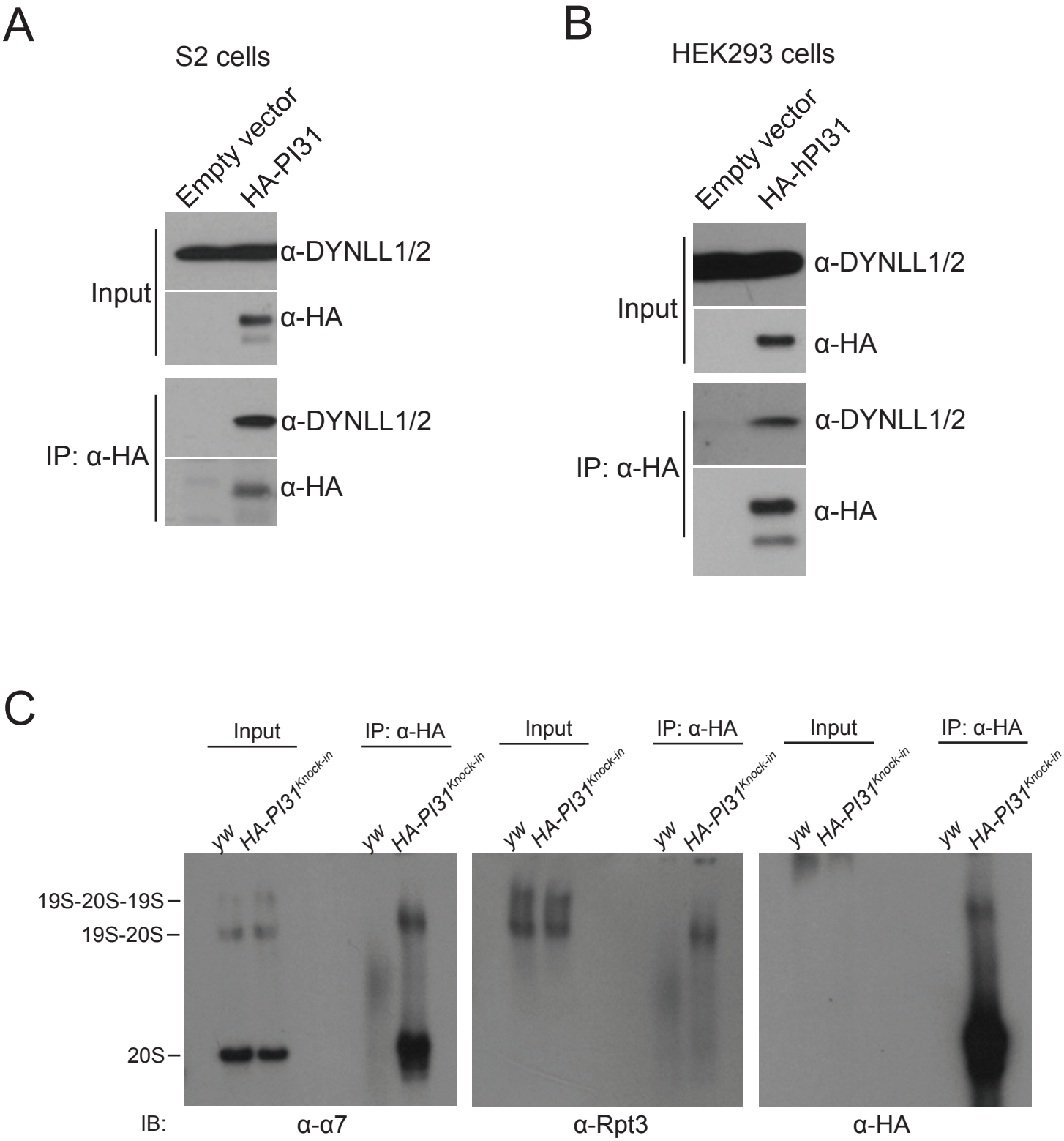
A
S2 cells
Empty vector
HA-PI31
Input
α-DYNLL1/2
α-HA
IP: α-HA
α-DYNLL1/2
α-HA
B
HEK293 cells
Empty vector
HA-hPI31
Input
α-DYNLL1/2
α-HA
IP: α-HA
α-DYNLL1/2
α-HA
C
Input
IP: α-HA
Input
IP: α-HA
Input
IP: α-HA
yw
HA-PI31Knock-in
19S-20S-19S
19S-20S
20S
IB:
α-α7
α-Rpt3
α-HA